https://doi.org/10.5194/essd-2026-628
Preprint. Discussion started: 10 August 2026

Open Access Earth System Science Data Discussions

Three decades of grassland canopy cover change in China (1990-2023) revealed by high-resolution mapping using extensive drone and Landsat data

Xuanhao Jiang[1,2,3], Tianyu Hu[1,2,3], Zhenying Huang[1,2], Zhiyao Tang[4], Leiyi Chen[1,2], Wenli Chen[2,5], Xiaoli Cheng[6], Yunxiang Cheng[7], Yuejun Fan[8], Ruiru Gao[9], Tiangang Gao[2,5], Yanming Gong[10], Yanpei Guo[4,11], Xiaokang Hu[12], Chengjun Ji[4], Liping Li[13], Shijin Li[14], Guofang Liu[15], Wanyin Luo[16], Hongyuan Ma[17], Wenhong Ma[7], Xiujuan Qiao[18], Chuangye Song[1,2], Guoyan Wang[19], Lei Wang[10], Qinggang Wang[20], Yonghui Wang[7], Zhong Wang[21], Xuejun Yang[1,2], Yan Yang[22], Yongchuan Yang[23], Xuehua Ye[1,2], Chunying Yin[24], Feihai Yu[25], Pujin Zhang[26], Shuren Zhang[2,5], Chengyang Zheng[4], Luhong Zhou[27], Yanjun Su[1,2,3,*]

[1]State Key Laboratory of Forage Breeding-by-Design and Utilization, Key Laboratory of Vegetation and Environmental Change, Institute of Botany, Chinese Academy of Sciences, Beijing, 100093, China

[2]China National Botanical Garden, Beijing, 100093, China

[3]University of Chinese Academy of Sciences, Beijing 100049, China

[4]Institute of Ecology, College of Urban and Environmental Sciences, and Key Laboratory for Earth Surface Processes of the Ministry of Education, Peking University, Beijing 100871, China

[5]Key Laboratory of Systematic and Evolutionary Botany, Institute of Botany, Chinese Academy of Sciences, Beijing 100093, China

[6]State Key Laboratory of Vegetation Structure, Function and Construction and Ministry of Education Key Laboratory for Transboundary Ecosecurity of Southwest China and Key Laboratory of Soil Ecology and Health in Universities of Yunnan Province, School of Ecology and Environmental Sciences, Yunnan University, Kunming 650091, China

[7]Ministry of Education Key Laboratory of Ecology and Resource Use of the Mongolian Plateau & Inner Mongolia Key Laboratory of Grassland Ecology, School of Ecology and Environment, Inner Mongolia University, Hohhot 010021, China

[8]Qinghai Agri-animal Husbandry Vocational College, Xining 812100, China

[9]School of Life Science, Shanxi Normal University, Shanxi 030031, China

[10]Xinjiang Institute of Ecology and Geography, Chinese Academy of Sciences, Urumqi 830011, China

[11]Yanchi Research Station, School of Soil and Water Conservation, Beijing Forestry University, Beijing 100083, China

[12]College of Agriculture and Biological Science, Dali University, Co-Innovation Center for Cangshan Mountain and Erhai Lake Integrated Protection and Green Development of Yunnan Province, Dali 671003, China

[13]Key Laboratory of Digital Earth Science, Aerospace Information Research Institute, Beijing 100094, China

[14]Key Laboratory of Plant Resources Conservation and Sustainable Utilization, South China Botanical Garden, Chinese Academy of Sciences, Guangzhou 510650, China

[15]College of Life and Environmental Sciences, Shaoxing University, Shaoxing 312000, China

[16]College of Aviation Meteorology, Civil Aviation Flight University of China, Sichuan 618307, China

[17]Northeast Institute of Geography and Agroecology, Chinese Academy of Science, Changchun 130102, China

https://doi.org/10.5194/essd-2026-628
Preprint. Discussion started: 10 August 2026

Open Access Earth System Science Data Discussions

[18]School of Life Science, Central China Normal University, Hubei 430079, China

[19]State Key Laboratory of Geohazard Prevention and Geoenvironment Protection, Chengdu University of Technology, Chengdu 610059, China

[20]College of Resources and Environmental Sciences, China Agricultural University, Beijing 100083, China

[21]Department of Ecology, College of Life Sciences, Wuhan University, Wuhan 430072, China

[22]Institute of Mountain Hazards and Environment, Chinese Academy of Sciences, Chengdu 610041, China

[23]College of Environment & Ecology, Chongqing University, Chongqing 400045, China

[24]CAS Key Laboratory of Mountain Ecological Restoration and Bioresource Utilization & Ecological Restoration and Biodiversity Conservation Key Laboratory of Sichuan Province, Chengdu Institute of Biology, Chinese Academy of Sciences, Chengdu 610041, China

[25]Institute of Wetland Ecology & Clone Ecology/Zhejiang Provincial Key Laboratory of Evolutionary Ecology and Conservation, Taizhou University, Taizhou 310000, China

[26]Institute of Grassland Research, Inner Mongolia Academy of Agricultural and Animal Husbandry Sciences, Hohhot 010031, China

[27]Key Laboratory for Humid Subtropical Eco-geographical Processes of the Ministry of Education, School of Geographical Sciences, Fujian Normal University, Fuzhou 350007, China

Correspondence to: Yanjun Su (ysu@ibcas.ac.cn)

Abstract. Long-term, high-resolution canopy cover data are essential for understanding grassland ecosystem dynamics and informing sustainable management. However, existing products are largely limited to coarse spatial resolutions, constraining their utility for high-precision, large-scale analyses. In this study, we collected over 16,000 drone image tiles (30 m × 30 m) from 2,144 sites across China and developed a machine learning model to produce a spatially seamless, 30 m annual dataset of national grassland canopy cover from 1990 to 2023 by integrating drone and Landsat-series imagery. The model achieves high predictive accuracy (R^2 = 0.73, RMSE = 18.4%) and robust temporal transferability (R^2 = 0.68, RMSE = 20.6%). Comparisons with existing large-scale products demonstrated significantly improved accuracy and reduced residual artifacts, underscoring the robustness of our approach across diverse grassland types and time periods. Spatiotemporal analysis indicated a multi-decadal mean canopy cover of 43.80 ± 18.69% across China's grasslands. Over the 34-year period, 41.76% of grasslands exhibited significant increases, 57.16% showed nonsignificant change, and 1.08% experienced significant declines. Climatic factors—including drought, precipitation, and temperature—emerged as the dominant drivers of canopy cover dynamics at the national scale, although their effects exhibited pronounced spatial heterogeneity. In contrast, anthropogenic pressures played a secondary role overall but could override climatic influences at local scales. Collectively, these findings, together with the long-term, high-resolution canopy cover dataset developed in this study, provide an essential basis for advancing the understanding of grassland ecosystem dynamics and for supporting evidence-based conservation and sustainable management strategies, particularly under intensifying climate change and increasing frequency of extreme events. The national grassland canopy cover dataset generated in this study is archived on Zenodo and can be freely downloaded from https://doi.org/10.5281/zenodo.20301123 (Jiang et al., 2026).

https://doi.org/10.5194/essd-2026-628
Preprint. Discussion started: 10 August 2026

1 Introduction

Among the most broadly distributed and ecologically important terrestrial ecosystems, grasslands play a critical role in carbon storage (Bai and Cotrufo, 2022), wind erosion control (Song et al., 2024), and livestock production (Maestre et al., 2022). In recent decades, however, grasslands have faced degradation and soil erosion under the combined pressures of the changing climate and expanding human activities, threatening their sustainable management and ecological restoration (Bardgett et al., 2021, Wang et al., 2022). To effectively monitor dynamics across grassland ecosystems, the development of large-scale, high-resolution, and long-term datasets on grassland growth status is urgently needed. Among the various indicators of grassland condition, canopy cover, defined as the fraction of ground vertically occupied by vegetation (Li et al., 2005), is a key metric widely used in assessments of grassland degradation (Bardgett et al., 2021), ecosystem health, and restoration effects (Jones et al., 2018). Nonetheless, achieving accurate, large-scale estimates of grassland canopy cover at fine spatial and temporal resolution is still a challenge.

In tradition, grassland canopy cover has been monitored over the long term mainly through field experiments (Tilman et al., 2001) and ground surveys within fixed grassland quadrats (Pywell et al., 2011). While such plot-level observations have revealed important ecological mechanisms in vegetation growth dynamics over time, they are spatially limited and lack broader representativeness, making their applicability at regional scales uncertain (Wiens, 1989). The advancement of remote sensing technologies, particularly the accumulation of long-term, periodic Earth observations, have given rise to several large-scale, long-term products, such as the MODIS Vegetation Continuous Fields (MODIS VCF) and the GEOV1/2 (Baret et al., 2013; DiMiceli et al., 2022). While these products capture broad canopy dynamics, their relatively coarse spatial resolution (~500 m) limits the detection of fine-scale changes, particularly in fragmented grasslands subject to intensive human disturbances (Daryaei et al., 2020).

The growing accessibility of medium- and high-resolution data, such as the Landsat and Sentinel missions, has made long-term, high-resolution grassland canopy cover mapping feasible (Andreatta et al., 2022; Zhou et al., 2024); yet, constrained by the limited spatiotemporal transferability of existing methods, most products remain confined to the regional scale. Spectral mixture analysis (SMA), for instance, is widely used for its operational flexibility and physically interpretable canopy cover estimates (Bian et al., 2017; Gao et al., 2020). However, SMA-based models often exhibit poor transferability because endmember composition varies substantially across regions and years, which limits their application to large-scale, long-term estimation of grassland canopy cover (Lewińska et al., 2025).

Machine learning algorithms, recognized for their computational efficiency and potential for spatial transferability (Ge et al., 2018), offer a powerful alternative for grassland canopy cover mapping (Lehnert et al., 2015). However, their performance is often constrained by the scarcity of field reference data, given the high labor intensity and cost of acquiring such data (Zhang et al., 2023). Furthermore, machine learning approaches are challenged by pronounced scale mismatches between ground quadrats (Dusseux et al., 2015) and satellite pixels, which can introduce substantial uncertainty into large-scale mapping (Hu et al., 2024; Woodcock and Strahler, 1987). Advances in drone technology offer a promising solution to address these

https://doi.org/10.5194/essd-2026-628
Preprint. Discussion started: 10 August 2026

limitations (Lyu et al., 2022). Very-high-resolution drone imagery, combined with image classification or deep learning techniques, enables accurate discrimination between grass and non-grass components, allowing efficient and non-destructive estimation of grassland canopy cover, which therefore substantially increases the availability of field reference data (Hu et al., 2024). Furthermore, by serving as a bridge between field observations and satellite data, the combination of drone and satellite imagery through machine learning algorithms has proven effective in mitigating scale mismatches and has been successfully applied to estimation at regional and even national scales (Chen et al., 2016). For instance, Hu et al. (2024) integrated extensive drone imagery with Sentinel-2 data via machine learning to generate a 10 m grassland canopy cover product across China, achieving an accuracy of 89%. However, most existing studies remain limited to single or discrete time points. Whether this approach offers sufficient temporal transferability to support the generation of a long-term, high-resolution grassland canopy cover product across China remains unvalidated.

Here, we aim to develop a temporally transferable machine learning model to generate an annual, 30 m resolution product of canopy cover for China's grasslands from 1990 to 2023, and to reveal its spatiotemporal dynamics and underlying drivers over the past three decades. To achieve this, we conducted an extensive drone survey across 2,144 grassland sites in China during 2021 and 2022. Based on this dataset, we developed a random forest (RF)-based regression model that integrates drone-derived canopy cover estimates with Landsat imagery to generate an annual canopy cover product for China's grasslands. To further assess the product's temporal accuracy, we additionally compiled 6,500 canopy cover observations from 30 sites spanning 2002 to 2022, derived from very-high-resolution satellite images. Finally, using linear regression and Shapley Additive Explanations (SHAP), we investigated the spatiotemporal patterns of China's grasslands and their underlying drivers, providing a robust foundation for assessing grassland ecosystem responses to climate and human factors.

2 Methods

2.1 Drone surveys

Drone imagery was acquired at 2,144 sampling sites across China over the June to September growing seasons of 2021 and 2022 (1,215 sites in 2021 and 929 in 2022), spanning seven major grassland types shown in Fig. 1. We selected these sites primarily by stratified random sampling, considering natural and anthropogenic factors, including vegetation zones, grassland types, human activity intensity, and field accessibility. At each site, a 100 m × 100 m grassland area was surveyed using drones following a crisscross boustrophedonic flight pattern, leaving a buffer of at least 10 m at the margins to limit edge effects. Imagery was captured using either a Phantom 4 Pro V2 or Phantom 4 RTK drone at a flight altitude of approximately 25-30 m. To reduce terrain-induced distortion when extracting canopy cover, orthorectified images with 0.01 m spatial resolution were generated from the raw drone photographs. Hu et al. (2024) provided the detailed workflow of the drone imagery acquisition and processing.

Orthorectified images exhibiting overexposure, blurring, or distortion were manually excluded, and the remaining high-quality images were clipped to 90 m × 90 m extents. Each clipped image was further subdivided into nine 30 m × 30 m tiles

https://doi.org/10.5194/essd-2026-628
Preprint. Discussion started: 10 August 2026

to match the resolution of Landsat imagery, producing 16,559 drone image tiles in total (9,575 from 2021 and 6,984 from 2022). To estimate grassland canopy cover, we applied the multilayer perceptron (MLP) model developed by Hu et al. (2024) to classify each pixel within these tiles as grass or non-grass. These processes, ultimately generated a high-resolution, drone-derived canopy cover reference dataset (Fig. 2a).

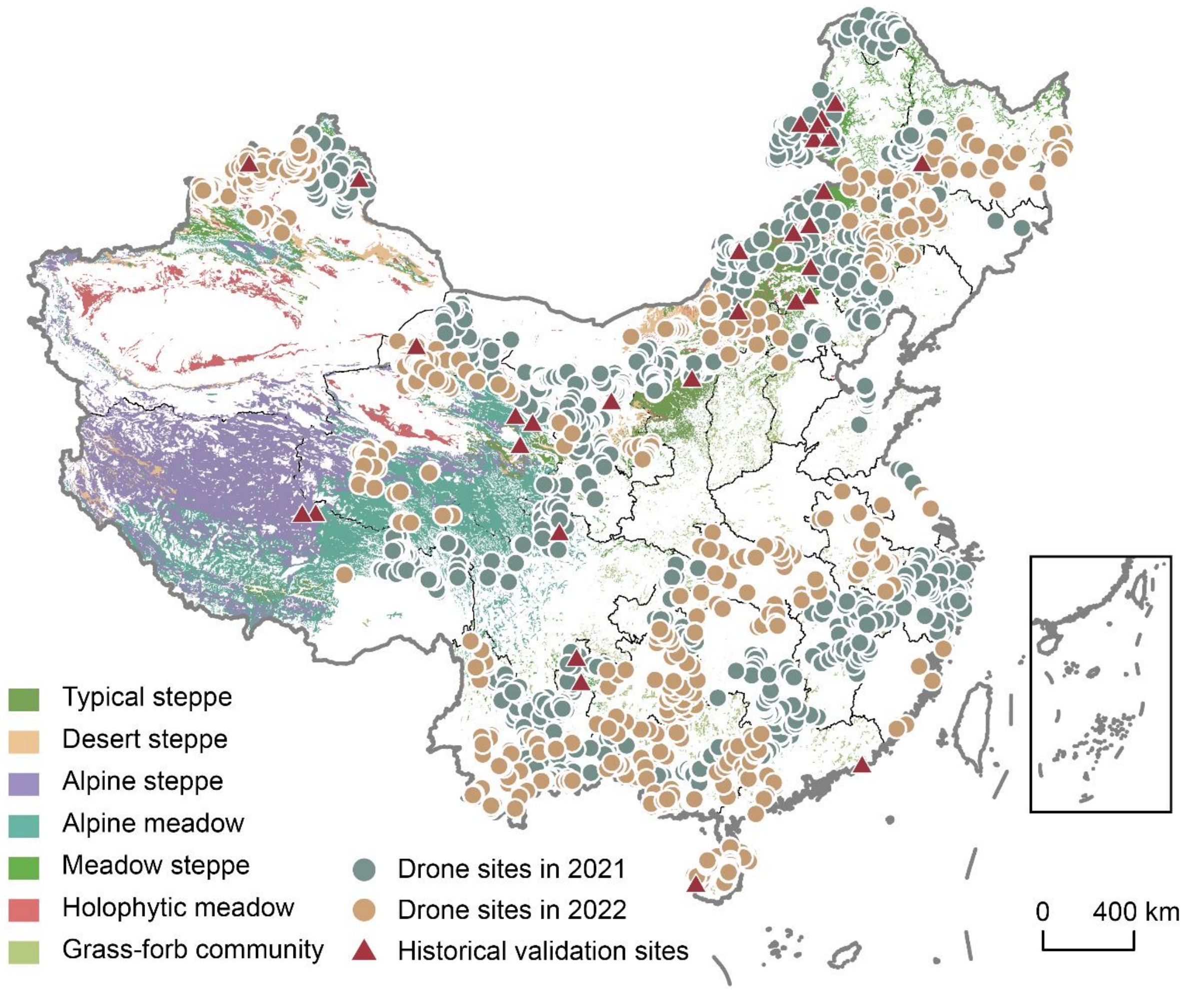

Fig. 1. Spatial distribution of drone survey sites and historical validation sites in relation to China's major grassland types. Grassland type information is sourced from the updated vegetation map of China (1:1,000,000) (Su et al., 2020).

2.2 Historical validation dataset

In addition to the drone-based reference dataset, we constructed a historical validation dataset to evaluate the temporal transferability of the developed RF-based canopy cover estimation model. To obtain reference canopy cover estimates spatially consistent with Landsat imagery, we acquired historical high-resolution (1-2 m) satellite imagery from Google Earth. Sites were selected according to three criteria: (1) representation of each major grassland type, with at least two sites per type; (2)

https://doi.org/10.5194/essd-2026-628
Preprint. Discussion started: 10 August 2026

availability of growing-season (April to September) imagery from at least two distinct years at each site; and (3) presence of a continuous grassland patch of no less than 300 m × 300 m. Due to the coarser spatial resolution of satellite imagery relative to drone imagery, automated classification with the MLP model may be less accurate. Therefore, grass and non-grass pixels were manually labeled for all historical satellite images (Fig. 2b). The labeled images were then aggregated into 30 m × 30 m tiles to produce reference canopy cover estimates.

Based on these criteria, we selected 30 historical validation sites across China (Fig. 1). From these sites, a total of 65 high-resolution historical satellite images (300 m × 300 m) covering 2002–2022 were obtained (Table 1). These images were subsequently divided into 6,500 tiles at 30 m resolution, providing reference canopy cover estimates for model validation.

Table 1 Number and acquisition years of historical high-resolution satellite images used for model validation, categorized by grassland type.

Grassland type	Number of images	Year
Typical steppe	12	2002, 2009-2011, 2013, 2015, 2017, 2019-2021
Desert steppe	5	2005, 2006, 2011, 2019
Alpine steppe	2	2009, 2020
Alpine meadow	9	2002-2003, 2009, 2010, 2013, 2017, 2019, 2020
Meadow steppe	15	2002, 2007, 2010, 2011, 2013, 2016-2020
Holophytic meadow	6	2007, 2012-2014, 2018, 2019
Grass-forb community	16	2012-2022

https://doi.org/10.5194/essd-2026-628
Preprint. Discussion started: 10 August 2026

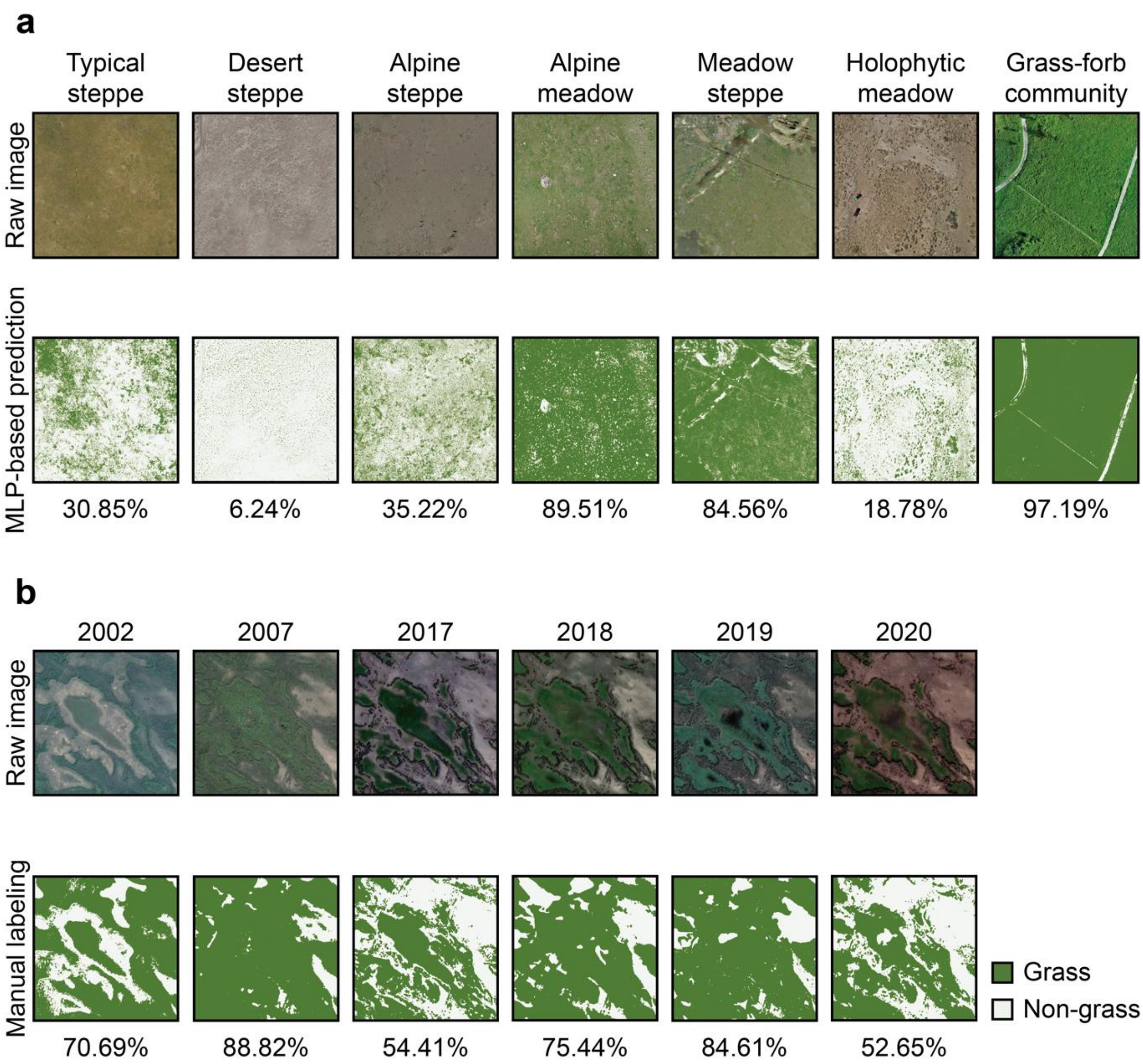

Fig. 2. Grass and non-grass pixels classified from drone and historical high-resolution imagery. (a) Classification of drone images using the multilayer perceptron (MLP) model developed by Hu et al. (2024). (b) Classification of historical high-resolution images based on manual labeling. Values beneath each image indicate the estimated grassland canopy cover.

2.3 Landsat imagery dataset and auxiliary data

In this study, time-series vegetation indices derived from Landsat imagery, along with topographic parameters, were used as the primary data sources for national-scale grassland canopy cover mapping. All available Landsat surface reflectance imagery over the study area from 1990 to 2023 was compiled (Table 2), including the five missions: Landsat 4 Thematic Mapper (TM), Landsat 5 TM, Landsat 7 Enhanced Thematic Mapper Plus (ETM+), and Landsat 8 and 9 Operational Land Imager (OLI/OLI-2). Imagery prior to 1990 was excluded due to limited availability and lower data quality. During the 1990-

2023 period, various sensor anomalies introduced image artifacts (Wulder et al., 2008), including detector failures in Landsat 5 TM (Fig. S1a), solid-state recorder bad block issue in Landsat 9 OLI-2 (Fig. S1b), shutter synchronization anomalies in Landsat 5 TM and Landsat 7 ETM+ (Fig. S1c), and sporadic band anomalies (Fig. S1d), which are non-negligible for long-term analyses. To ensure data quality, we applied a rigorous filtering protocol: (1) constraining surface reflectance to the range 0-1 (Cai et al., 2024); (2) masking cloud and cloud shadow pixels via the Quality Assessment (QA) band (Zhu et al., 2015); (3) retaining only images with a per-image standard deviation of the green chlorophyll vegetation index below 10; (4) manually excluding images with significant visual artifacts; (5) removing pixels affected by sensor anomalies based on the QA_RADSAT band; and (6) eliminating statistical outliers using the three-sigma rule (Barnett and Lewis, 1994). While the TM, ETM+, and OLI sensors share broadly similar spectral bands, slight differences in spectral response functions exist. To reduce inter-sensor variability, we harmonized the dataset using OLI imagery as the reference and calibrating TM/ETM+ data with the transformation coefficients from Roy et al. (2016). Visual inspection confirmed these corrections effectively yielded a high-quality long-term dataset largely free of known artifacts (Fig. S1).

Table 2 Overview of Landsat data sources used from 1990 to 2023. TM, ETM+, and OLI refer to Thematic Mapper, Enhanced Thematic Mapper Plus, and Operational Land Imager, respectively.

Year	Data source	Number of tiles
1990-1993	Landsat-4 TM, Landsat-5 TM	48,203
1994-1998	Landsat-5 TM	57,560
1999-2012	Landsat-5 TM, Landsat-7 ETM+	310,618
2013-2021	Landsat-7 ETM+, Landsat-8 OLI	310,366
2022-2023	Landsat-8 OLI, Landsat-9 OLI-2	74,770

Topographic information was derived from the 30 m Shuttle Radar Topography Mission (SRTM) v3 digital elevation model (DEM) (Farr et al., 2007). In addition to Landsat and topographic data, land cover data were used in grassland canopy cover mapping to define grassland extent and type. Specifically, the spatial extent of grasslands was derived from the 30 m annual land-cover dataset of China covering 1990-2024 (Yang and Huang, 2021). To analyze the spatial distribution of grassland canopy cover nationwide, we further obtained grassland-type information from the updated vegetation map of China (1:1,000,000) (Su et al., 2020).

To identify what drives canopy cover dynamics across China's grasslands, we further compiled a time-series dataset of climate and human activity variables (Table 3). Climate variables included precipitation, temperature, and the standardized precipitation-evapotranspiration index (SPEI). Monthly precipitation and temperature data were sourced from the ERA5-Land product (0.1° resolution), which is a widely used reanalysis dataset integrating meteorological observations with numerical models (Muñoz-Sabater et al., 2021), and subsequently aggregated to annual means. Drought was characterized using the 12-month SPEI from the global SPEI database (0.5° resolution; Vicente-Serrano et al., 2010), which captures combined anomalies in precipitation and potential evapotranspiration and responds sensitively to temperature (Beguería et al., 2014). To quantify anthropogenic influences, we selected two variables: the human modification index (HMI) and a grazing index. HMI is a comprehensive indicator of cumulative human pressures on terrestrial ecosystems (Kennedy et al., 2019). We derived this

https://doi.org/10.5194/essd-2026-628
Preprint. Discussion started: 10 August 2026

metric from the 1990-2022 Global Human Modification v3 dataset, which provides data at a 300 m spatial resolution at five-year intervals (Theobald et al., 2025). The grazing index was extracted from a long-term, high-resolution dataset that integrates field observations with a grassland growth model (Wang et al., 2024). This dataset provides estimates at 0.1° resolution for 1980-2000 and 0.0025° resolution for 2001-2022. To characterize the long-term variations over the past three decades, we calculated the temporal trend from 1990 to 2020 for each climate and human activity variable. To ensure spatially consistency with the developed national grassland canopy cover dataset, all variables were resampled to 30 m by bilinear interpolation.

Table 3 Overview of other auxiliary data used in this study. Note that SPEI and HMI represent standardized precipitation-evapotranspiration index and human modification index, respectively.

Category	Variable	Spatial Res.	Reference
Topography	Elevation	30 m	Farr et al., 2007
	Slope		
	Aspect		
Land cover	Grassland extent	30 m	Yang and Huang, 2021
Vegetation map	Grassland type	Vector	Su et al., 2020
Climate	Temperature	0.1°	Muñoz-Sabater et al., 2021
	Precipitation		
	SPEI	0.5°	Vicente-Serrano et al., 2010
Anthropogenic	HMI	300 m	Theobald et al., 2025
	Grazing	0.1° for 1980-2000 0.0025° for 2001-2022.	Wang et al., 2024

2.4 Time-series mapping of national grassland canopy cover

Using the drone-derived reference dataset and satellite observations, we generated an annual, 30 m resolution dataset of canopy cover for China's grasslands from 1990 to 2023. The overall workflow comprised three main steps (Fig. S2): (1) extracting feature datasets, including Landsat-derived vegetation indices and topographic parameters, using the Google Earth Engine (GEE) platform; (2) developing an RF regression model by integrating the drone-based reference data with these satellite-derived features and applying the trained model within GEE to produce a spatially seamless, 30 m annual dataset of national grassland canopy cover; and (3) evaluating model performance, temporal transferability, and per-pixel uncertainty. The following sections provide detailed information on each of these steps.

2.4.1 Feature extraction

To map multi-year grassland canopy cover across China, we selected vegetation indices and topographic parameters as input features for the estimation model. Five vegetation indices were derived from the 30 m Landsat imagery: the Normalized

Difference Vegetation Index (NDVI), Difference Vegetation Index (DVI), Normalized Difference Water Index (NDWI), Green Chlorophyll Vegetation Index (GCVI), and Soil Adjusted Vegetation Index (SAVI), which are widely recognized, well-validated proxies for biophysical properties, effectively capturing vegetation growth status, canopy moisture, and chlorophyll content (Glenn et al., 2008). To further reduce cloud contamination, annual Landsat imagery was aggregated using maximum value composites (MVC), which typically represent peak vegetation growth conditions (Holben, 1986; Taddei, 1997), and the indices were derived from the composited Landsat imagery dataset. In addition, to ensure temporal consistency between Landsat features and the drone-based reference data used, indices were further extracted from Landsat scenes acquired closest to the acquisition dates of drone or historical imagery. After feature extraction, tiles containing missing data or invalid NDVI values (i.e., NDVI < 0 or > 1) were excluded. Ultimately, 13,680 image tiles were retained in the drone-based dataset, along with 5,416 tiles in the historical validation dataset.

In addition to vegetation indices, three topographic variables—elevation, slope, and aspect—were obtained from the SRTM v3 DEM as key input features for national-scale grassland canopy cover mapping, given their fundamental role in regulating hydrothermal processes.

2.4.2 Model construction and dataset mapping

We used the RF algorithm (Breiman, 2001), a computationally efficient and robust machine-learning framework in remote sensing that is well suited to potentially collinear predictors such as Landsat-derived spectral indices. To generate long-term grassland canopy cover maps across China, we developed an RF regression model trained on the drone-derived reference dataset, using the aforementioned vegetation indices and topographic parameters as input features. The key hyperparameters were set following a manual trial-and-error approach (Table S1). We assessed each variable's relative importance with the mean decrease in impurity, which measures the total reduction in target variance contributed by each feature across all decision trees within the RF ensemble (Louppe et al., 2013). All computational procedures were implemented in Python with the *RandomForestRegressor* module from *scikit-learn* library.

To generate a long-term, 30 m annual dataset of annual peak grassland canopy cover across China, we implemented the trained model, using five vegetation indices derived from Landsat MVCs and three topographic parameters as input features. The resulting canopy cover estimates were further masked using annual grassland extents derived from land cover data (Yang and Huang, 2021), thereby producing the final national maps of annual grassland canopy cover across China from 1990 to 2023. All data compositing, feature extraction, and predictive mapping processes were conducted on the GEE platform.

2.4.3 Accuracy and uncertainty assessment

To validate the generated national canopy cover maps, we evaluated both the accuracy and temporal transferability of the RF regression model. First, model predictive accuracy was assessed using the retained 30% independent drone reference dataset (n = 4104). Second, model temporal transferability was evaluated using an independent historical reference dataset (n = 5416). To characterize whether model performance remained stable across different periods, the historical reference dataset was further stratified into four periods (2002-2007, 2008-2012, 2013-2017, and 2018-2022). Two statistical metrics were calculated to quantify the model performance by comparing model predictions with the corresponding validation observations, including the coefficient of determination (R^2) and the root mean squared error (RMSE),

$$R^2 = 1 - \frac{\sum_{i=1}^{n}(\mathrm{cover}_i - \widehat{\mathrm{cover}}_i)^2}{\sum_{i=1}^{n}(\mathrm{cover}_i - \overline{\mathrm{cover}}_i)^2} \tag{1}$$

$$\mathrm{RMSE} = \sqrt{\frac{1}{n}\sum_{i=1}^{n}(\mathrm{cover}_i - \widehat{\mathrm{cover}}_i)^2} \tag{2}$$

where $\widehat{\mathrm{cover}}_i$ is the model prediction, cover_i is the observation, $\overline{\mathrm{cover}}_i$ is the mean of the observation values, and n is the number of samples in the training or validation dataset.

To estimate the uncertainty of the national grassland canopy cover product, we used a five-fold cross-validation ensemble. The drone-derived canopy cover reference dataset was randomly divided into five equal subsets; each subset was held out in turn while an RF regression model was fitted to the other four, producing five independent models. Each model was applied to 2021, the year with the most drone sampling sites, and the per-pixel standard deviation across the five predictions was taken as the uncertainty of the estimated canopy cover (Cai et al., 2024).

2.5 Analysis of long-term grassland canopy cover dynamics of China

To quantify the long-term dynamics of grassland canopy cover across China, we performed pixel-wise linear regression using the developed time-series canopy cover dataset. For each pixel, the regression slope captured both the direction and rate of canopy cover change, while the associated p-value indicated the statistical significance of the trend. Using these two metrics, we grouped canopy cover dynamics into three trajectory categories: significant gain (slope > 0, $p < 0.05$), significant loss (slope < 0, $p < 0.05$), and nonsignificant change ($p > 0.05$). Moreover, we employed an extreme gradient boosting (XGBoost) model to assess the contributions of climatic and anthropogenic drivers to grassland canopy cover dynamics (Chen and Guestrin, 2016). Specifically, the model was trained to predict the regression slope from the five variables described above, with a configuration of 2000 trees and a maximum tree depth of 6 (Table S2). Notably, to optimize computational efficiency, a 10% random sample of the full dataset was utilized to train the XGBoost model. Preliminary tests confirmed that the further increases in training data yielding negligible improvements in predictive performance (Fig. S3). Predictor contribution at the pixel level was quantified using SHAP values (Mersha et al., 2024). Based on these values, we mapped the dominant driver of each pixel, defined as the predictor with the highest absolute SHAP value. Nationally, each factor was ranked by the mean absolute SHAP value across all pixels. Finally, SHAP dependence plots, fitted with a locally weighted scatterplot smoothing, were generated to visualize the marginal effects and directional influences of individual drivers. It should be noted that all temporal trend analyses were restricted to stable pixels that maintained grassland status for a minimum of 30 years, to eliminate the confounding effects of land-use change. All model training and analyses described above were implemented in Python using the *xgboost* package.

https://doi.org/10.5194/essd-2026-628
Preprint. Discussion started: 10 August 2026

3 Results

3.1 The accuracy and temporal transferability of canopy cover estimation model

Building upon the extensive drone-derived reference dataset and satellite observations, we developed an RF model for time-series canopy cover mapping. Overall, vegetation indices exhibited the highest influence on canopy cover estimation, accounting for more than 90% of the total variable importance (Fig. 3). Among the vegetation indices, NDVI was the most influential predictor (25.68%), followed by NDWI (23.47%), GCVI (18.45%), SAVI (13.94%), and DVI (9.55%) (Fig. 3). By contrast, topographic variables were of limited relative importance; elevation contributed more than slope and aspect, yet the three together explained only a minor share of the overall importance (Fig. 3).

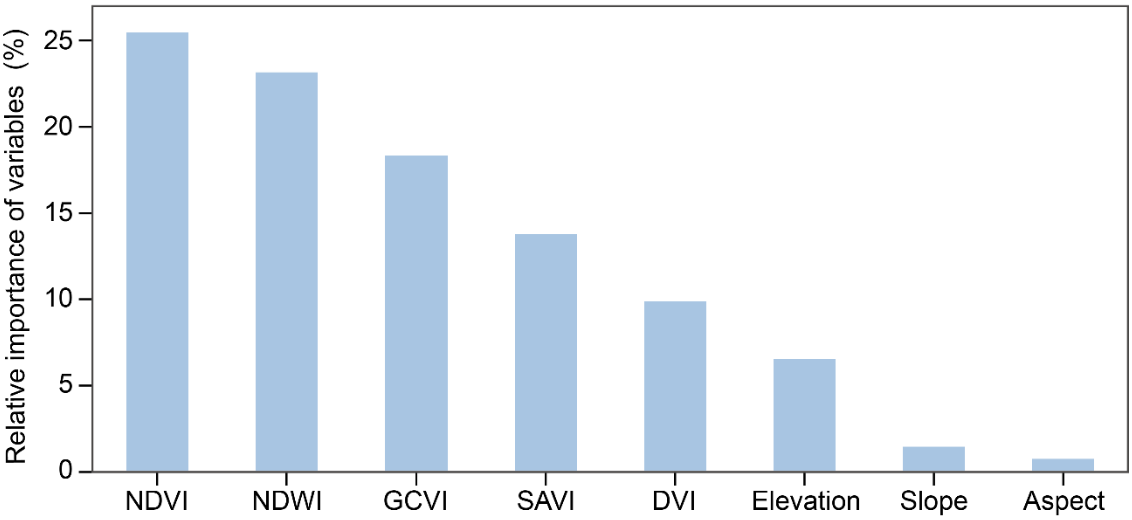

Fig. 3. Relative importance of the eight variables in grassland canopy cover estimation model. Vegetation indices are abbreviated as follows: NDVI, Normalized Difference Vegetation Index; NDWI, Normalized Difference Water Index; GCVI, Green Chlorophyll Vegetation Index; SAVI, Soil Adjusted Vegetation Index; DVI, Difference Vegetation Index.

Model validation demonstrated the strong predictive accuracy of the model. When evaluated against the drone-based grassland canopy cover reference dataset, the model explained 73% of the observed variance (R^2 = 0.73) with an RMSE of 18.4%, and the predicted values were closely aligned with the 1:1 reference line (Fig. 4a), indicating that the model effectively captures canopy cover variability across different grassland types. Although validation with the historical dataset revealed a slight degradation in temporal transferability (R^2 = 0.68, RMSE = 20.6%), the model remained robust (Fig. 4b), highlighting its predictive stability across grassland types and through different years. This robustness was further supported by the period-stratified validation (Fig. 4c-f), in which R^2 ranged from 0.55 to 0.71 and RMSE from 19.8% to 21.5% across the four periods (2002-2007, 2008-2012, 2013-2017, and 2018-2022). Although agreement was slightly lower during 2013-2017 (Fig. 4e), the model maintained comparable accuracy across all periods, indicating stable temporal transferability throughout the historical validation record. Notably, all validation datasets exhibited a consistent pattern: canopy cover was overestimated under sparse-

https://doi.org/10.5194/essd-2026-628
Preprint. Discussion started: 10 August 2026

to-moderate vegetation and underestimated under dense cover (Fig. 4). Nevertheless, the relatively small residuals suggest that the RF model provided reliable estimates across diverse temporal and spatial conditions.

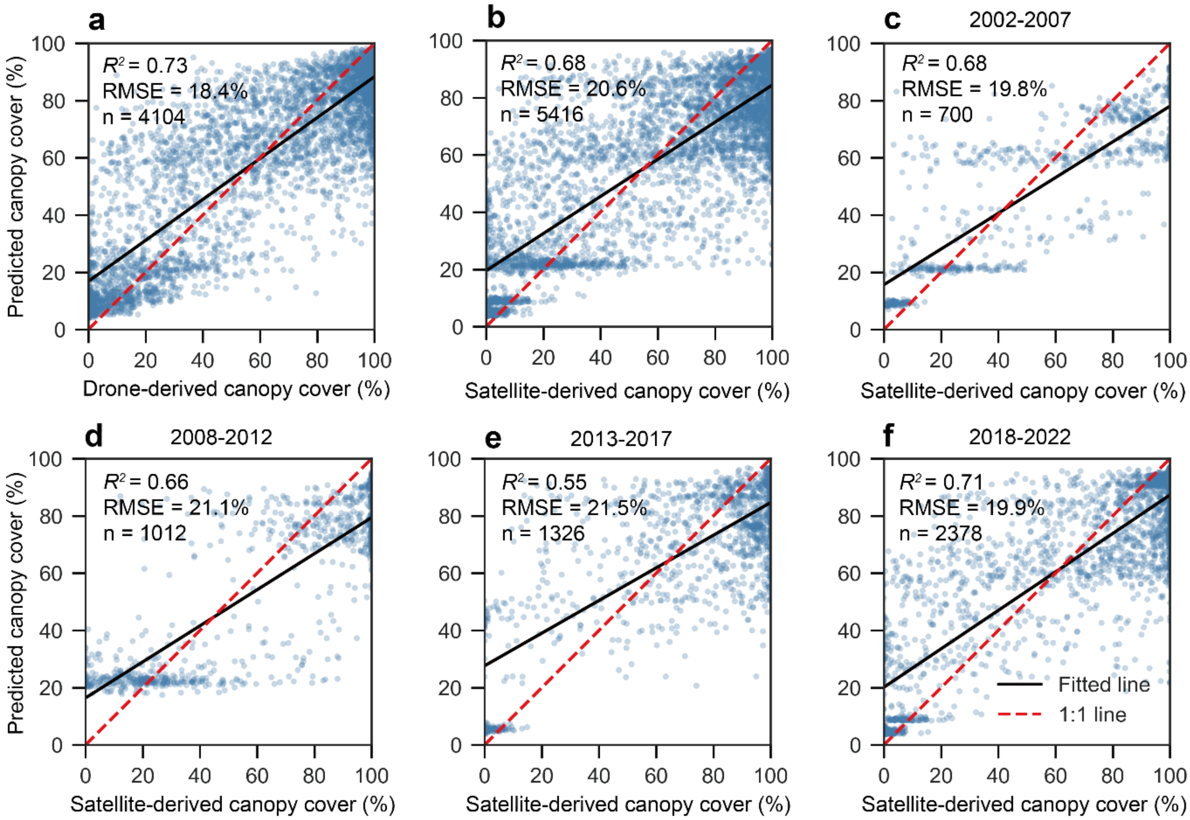

Fig. 4. Predictive accuracy and temporal transferability assessment of the random forest (RF) model. (a) Validation against the retained 30% drone-derived reference dataset; (b) overall validation against the historical satellite-derived reference dataset, with (c–f) results for 2002-2007, 2008-2012, 2013-2017, and 2018-2022. R^2 and RMSE represent the coefficient of determination and root-mean-squared error, respectively; n is the sample size.

3.2 The spatiotemporal dynamics of China's grassland canopy cover from 1990 to 2023

Using the RF-based regression model and the GEE platform, we generated 30 m wall-to-wall annual maps of canopy cover for China's grasslands from 1990 to 2023 (Fig. 5). Nationally, grassland canopy cover exhibited a pronounced southeast-northwest decreasing gradient, with higher canopy cover in the warm, humid southeastern regions and progressively lower canopy cover toward the cold, arid northwest (Fig. 5). This spatial pattern remained consistent throughout the study period (Fig. 5). The 34-year mean grassland canopy cover was 43.80%, with a standard deviation of 18.69%, indicating substantial spatial heterogeneity (Fig. 6a).

https://doi.org/10.5194/essd-2026-628
Preprint. Discussion started: 10 August 2026

314

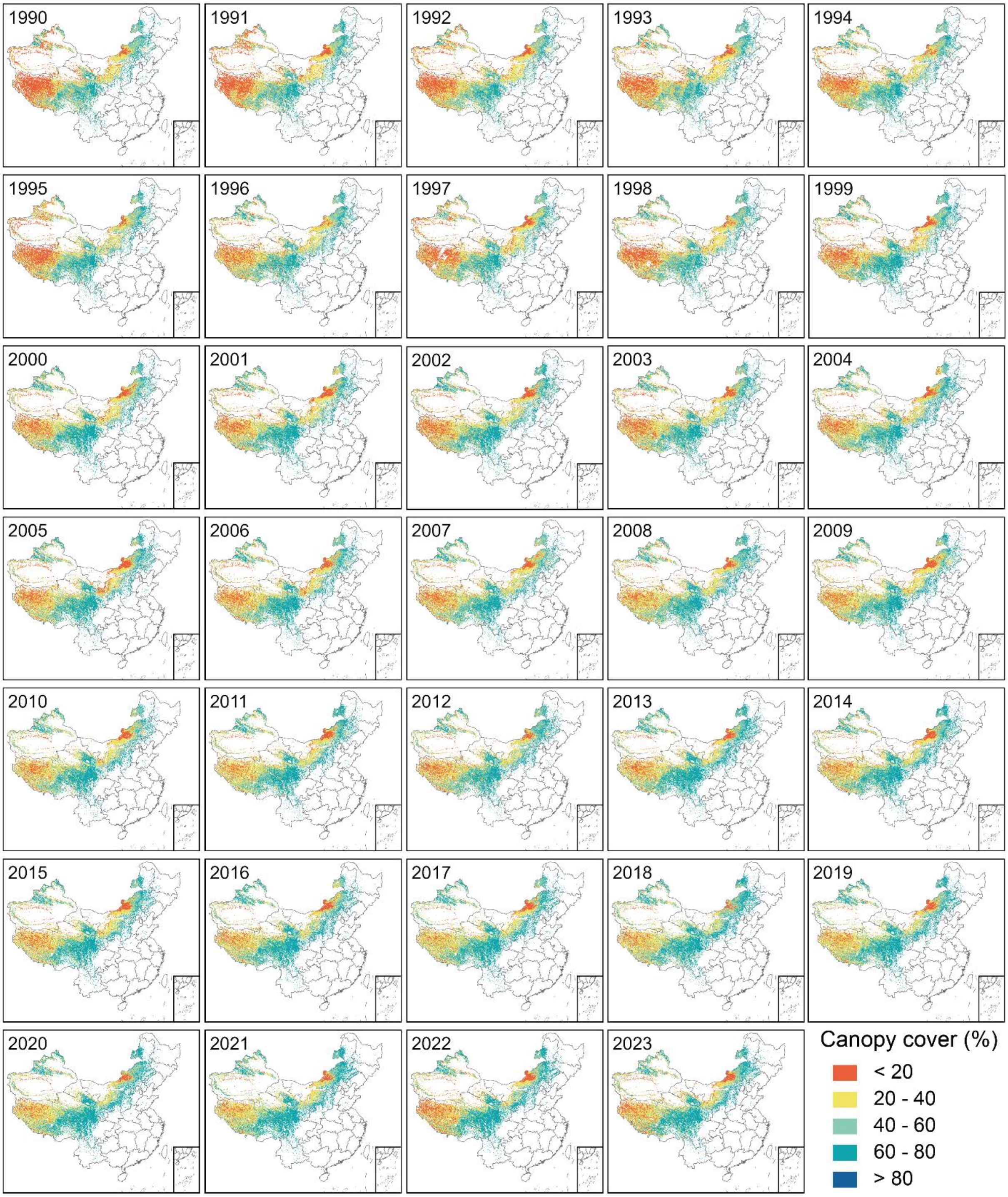

315

316 **Fig. 5.** An overview of annual grassland canopy cover map of China from 1990 to 2023.

https://doi.org/10.5194/essd-2026-628
Preprint. Discussion started: 10 August 2026

Canopy cover distributions varied significantly among grassland types (Fig. 6b). Grass-forb community and meadow steppe showed the highest canopy cover (exceeding 60%), while alpine meadow and typical steppe showed intermediate levels. In contrast, holophytic meadow, desert steppe and alpine steppe generally recorded values below 35% (Fig. 6b). Variability also differed among grassland types, with holophytic meadows exhibiting the greatest variability and grass-forb communities the least (Fig. 6b). At the provincial scale, 34-year mean canopy cover exhibited substantial spatial heterogeneity, ranging from 34.32% in Xizang to 71.55% in Heilongjiang (Fig. 6c). Eastern provinces, including Heilongjiang, Beijing, Shandong, and Liaoning, exhibited consistently high canopy cover with relatively low variability (Fig. 6c), reflecting the dominance of grass-forb communities or meadow steppe. In contrast, the western provinces—Gansu, Qinghai, Inner Mongolia, Xinjiang, Ningxia, and Xizang—showed lower overall canopy cover but higher spatiotemporal variability (Fig. 6c), corresponding to the widespread distribution of alpine, desert, and typical steppe. Provinces with mixed grassland types, such as Sichuan, Guizhou, and Yunnan, exhibited intermediate canopy cover levels and moderate variability (Fig. 6c).

https://doi.org/10.5194/essd-2026-628
Preprint. Discussion started: 10 August 2026

Open Access Earth System Science Data Discussions

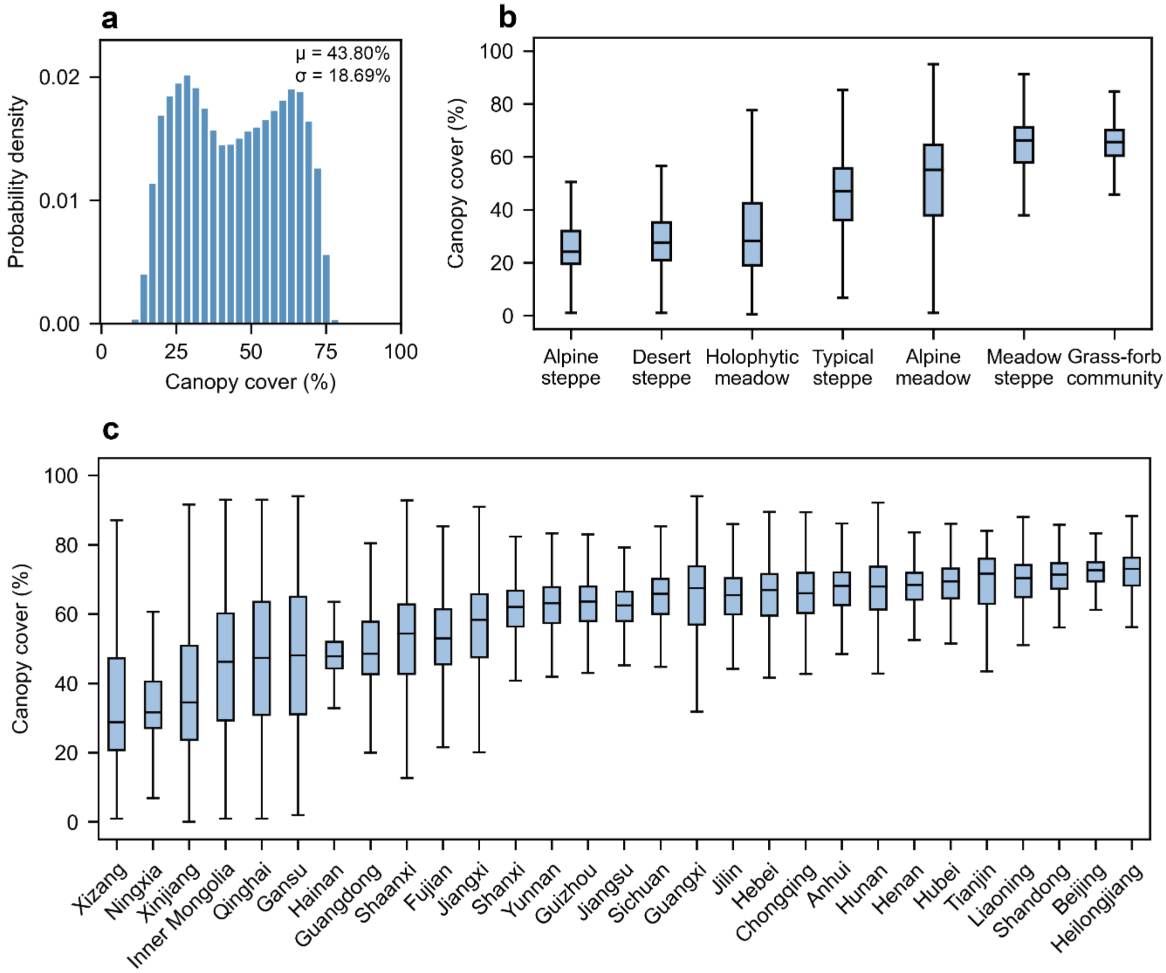

Fig. 6. (a) Histogram of the 34-year mean grassland canopy cover across China. (b) Boxplots of the 34-year mean China's grassland canopy cover across major grassland types. (c) Boxplots of the 34-year mean China's grassland canopy cover across provinces. Provinces with a grassland area of less than 100 km² are excluded.

Over the past three decades, most grasslands in China experienced either significant gain or remained relatively stable, while only a small proportion exhibited significant declines (Fig. 7a). Nationwide, 41.76% of grasslands showed significant increases in canopy cover, 57.16% exhibited nonsignificant change, and only 1.08% experienced significant declines (Fig. 7b), indicating an overall improvement of grassland condition throughout the study period. Regions with significant canopy cover increases were primarily concentrated in the Tibetan Plateau, the Loess Plateau, and parts of Xinjiang. Canopy cover dynamics varied substantially across provinces (Fig. 7c). Among all provinces, Qinghai, Shaanxi, Xizang, and Xinjiang had the highest proportions of significant increase. In contrast, Inner Mongolia predominantly exhibited nonsignificant changes in canopy cover, and displayed the most prominent proportion of localized grassland canopy cover loss among the analyzed provinces.

https://doi.org/10.5194/essd-2026-628
Preprint. Discussion started: 10 August 2026

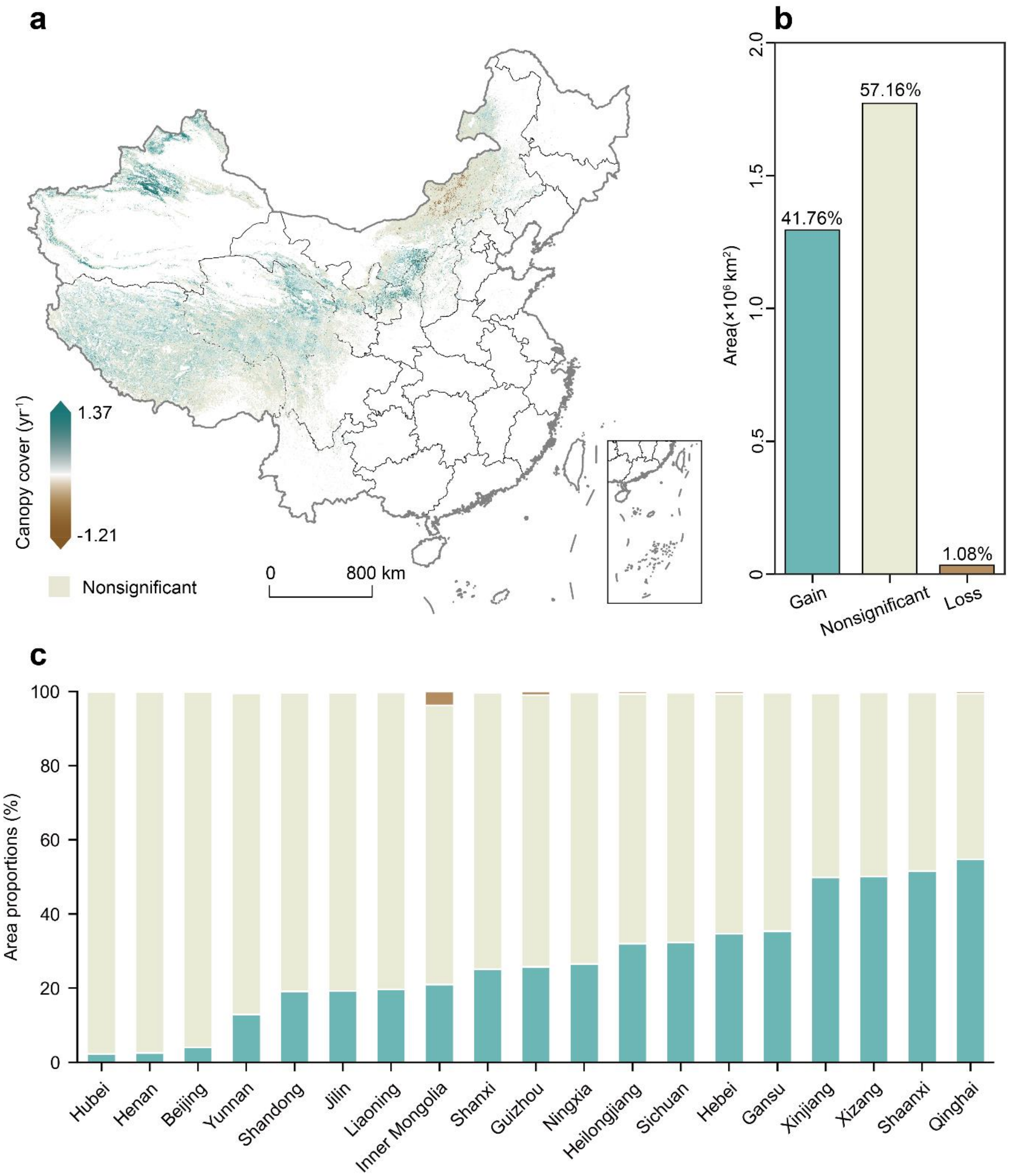

Fig. 7. Trends in canopy cover change across China's grassland from 1990 to 2023. (a) Spatial distribution of the regression slope, representing canopy cover change. (b) Areas with increasing, nonsignificant, and decreasing canopy cover trends across China. (c) Proportional area of canopy cover trends by province in China. Provinces with a grassland area of less than 100 km² are excluded.

https://doi.org/10.5194/essd-2026-628
Preprint. Discussion started: 10 August 2026

3.3 Drivers of grassland canopy cover dynamics across China

Overall, the temporal trends of the five selected climatic and anthropogenic variables explained 36% of the variation in grassland canopy cover dynamics across China, as quantified by the XGBoost model (Fig. 8a). Among these variables, climatic factors exerted a substantially stronger influence on canopy cover changes than anthropogenic factors, with drought conditions emerging as the most important driver (Fig. 8a). Drought accounted for 49.73% of grassland canopy cover change nationwide, particularly across the extensive northern and northeastern pastoral regions (Fig. 8b). Following drought, precipitation and temperature ranked second and third in importance (Fig. 8a), accounting for 29.40% and 13.73% of China's grassland change, respectively (Fig. 8b). Precipitation played a dominant role in the Loess Plateau, central-eastern Qinghai-Tibet Plateau, and portions of Xinjiang and Inner Mongolia. In contrast, the regions dominated by temperature were more fragmented, appearing sporadically across the Qinghai-Tibet Plateau and the Loess Plateau. Among the two anthropogenic variables, grazing intensity exhibited slightly greater importance than HMI (Fig. 8a), accounting for 6.69% and 0.64% of China's grassland canopy cover change, respectively (Fig. 8b). Rather than dominating extensive contiguous areas, the anthropogenic drivers were primarily manifested as scattered patches across Xinjiang and the Qinghai-Tibet Plateau. Notably, as one of China's key pastoral regions, Qinghai-Tibet Plateau exhibited grassland canopy cover dynamics driven by a complex interplay of multiple factors. Unlike other regions, no single variable exerted clear dominance; instead, temperature variations, moisture availability, and localized grazing pressures jointly shaped canopy cover dynamics across the region.

https://doi.org/10.5194/essd-2026-628
Preprint. Discussion started: 10 August 2026

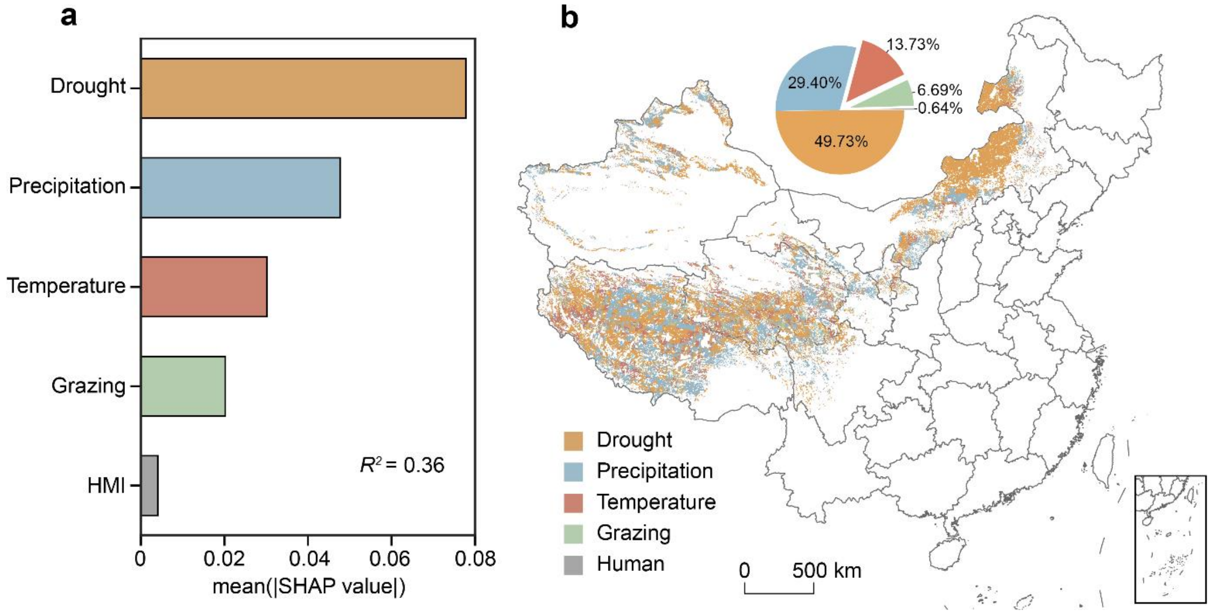

Fig. 8. Relative importance of climatic and anthropogenic factors to grassland canopy cover change. (a) Overall feature importance evaluated by mean absolute Shapley Additive Explanations (SHAP) values derived from the extreme gradient boosting model. (b) Spatial distribution of the dominant driving factors, defined as the driver with the highest absolute SHAP value for each pixel. The inset pie chart illustrates the areal proportions of these dominant drivers across the study region.

Temporal trends in climatic and anthropogenic drivers exerted complex and dynamic influences on grassland canopy cover. Overall, SPEI exhibited a slight decreasing trend across China's grasslands (Fig. S4); as the SPEI trend increased, its impact on canopy cover gradually shifted from an inhibitory effect to a neutral, stable state (Fig. 9a). Precipitation showed an overall declining trend (Fig. S5); with increasing precipitation trends, its influence transitioned from a fluctuating pattern to a negative effect (Fig. 9b). Temperature demonstrated a warming trend (Fig. S6), and as warming intensified, its impact shifted from positive facilitation to slightly negative (Fig. 9c). Among anthropogenic factors, grazing intensity exhibited a slight upward trend (Fig. S7). As grazing trends shifted from negative to positive, their effect on canopy cover transitioned sharply from positive to strongly negative (Fig. 9d). HMI showed a slight increasing trend (Fig. S8); with further increases, its influence on canopy cover shifted from neutral to a significant positive driving force (Fig. 9e).

https://doi.org/10.5194/essd-2026-628
Preprint. Discussion started: 10 August 2026

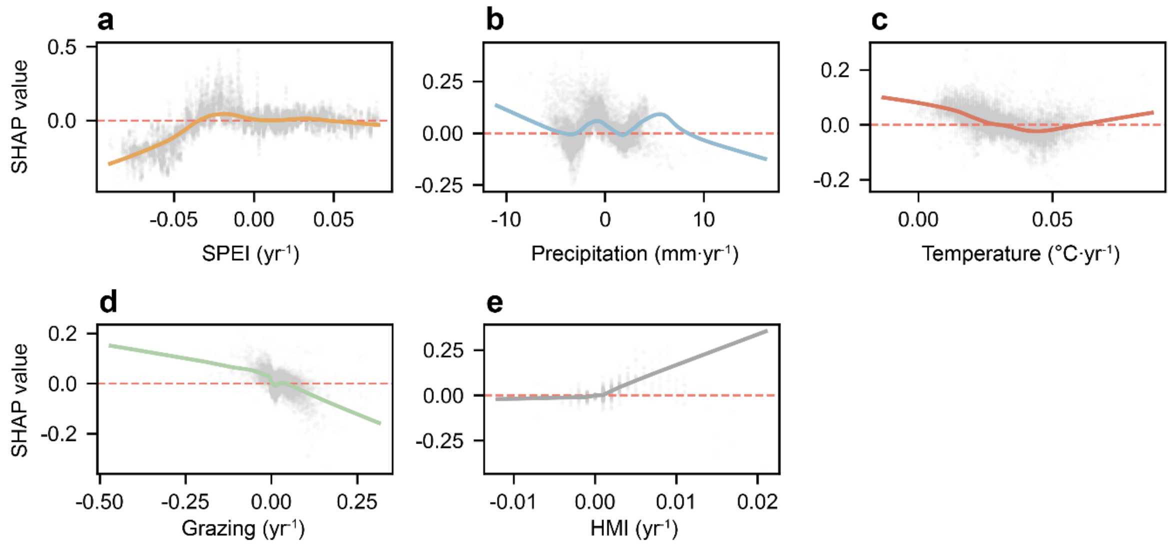

Fig. 9. Effects of temporal trends in climatic and anthropogenic drivers on grassland canopy cover dynamics. The influences of five factors (a-e: trends in standardized precipitation–evapotranspiration index (SPEI), precipitation, temperature, grazing intensity, and human modification index (HMI) are quantified using SHAP values. The red dashed line represents the zero SHAP value.

4 Discussion

4.1 High-resolution time-series mapping of large-scale grassland canopy cover

An RF-based grassland canopy cover estimation model with high precision and robust temporal transferability is essential for long-term, large-scale grassland canopy cover mapping. Benefiting from extensive drone-derived reference data that spatially matches satellite observations (Hu et al., 2024), our RF regression model demonstrates both high prediction accuracy and robust temporal transferability (Fig. 4a, b). Incorporating multi-year drone imagery across a broader spatial distribution further enhances data representativeness, thereby improving the model's overall performance (Fig. S9). Nevertheless, the RF-based grassland canopy cover estimation model shares a common limitation with other machine learning-based vegetation retrieval methods: a tendency to slightly overestimate canopy cover under sparse-to-moderate vegetation areas and underestimated it under dense cover (Gessner et al., 2013; Hu et al., 2024). Under high canopy cover, NDVI and related vegetation indices typically saturate (Hatfield et al., 1985), weakening the spectral discrimination of dense vegetation and causing systematic underestimation. Conversely, in low-cover regions, spectral signals are heavily influenced by soil background and mixed pixels (Huete, 1988), which artificially inflate vegetation index values and lead to overestimation (Xiao and Moody, 2005). Future studies could mitigate this bias by integrating structural information derived from lidar observations (Dubayah et al., 2020).

Consistent with previous research (Hu et al., 2024), vegetation indices such as NDVI emerged as the dominant predictors, substantially outperforming topographic parameters (Fig. 3). This reflects their ability to directly capture dynamic biophysical

https://doi.org/10.5194/essd-2026-628
Preprint. Discussion started: 10 August 2026

properties, such as vegetation greenness (Huete et al., 2002; Tucker, 1979), leaf water content (Gao, 1996; Hunt Jr. and Rock, 1989), and chlorophyll concentration (Gitelson and Merzlyak, 1994). In contrast, topographic parameters primarily represent static environmental constraints and therefore provide limited explanatory power for interannual variability in canopy cover. Notably, although grassland canopy cover is highly sensitive to precipitation and temperature (Smith et al., 2024; You et al., 2025), we intentionally excluded climatic variables from the final RF model to avoid multicollinearity in subsequent analyses of canopy cover drivers. A comparative experiment showed that incorporating climate predictors surprisingly reduced temporal transferability by 11.5% (R^2 = 0.61; RMSE = 22.6%) (Fig. 10a) and exacerbated systematic biases (Fig. 10b, c). This decline in performance is likely attributable to the limited temporal coverage of the training data. Specifically, climate change has intensified over the past three decades, leading to more frequent extreme events (Chen et al., 2025; Yuan et al., 2023), whereas the drone surveys conducted in 2021-2022 do not adequately capture the long-term climatic baseline or interannual variability of the full 1990-2023 study period (Fig. S10). Consequently, incorporating climate variables into the model compromises its temporal transferability when extrapolating to historical periods.

https://doi.org/10.5194/essd-2026-628
Preprint. Discussion started: 10 August 2026

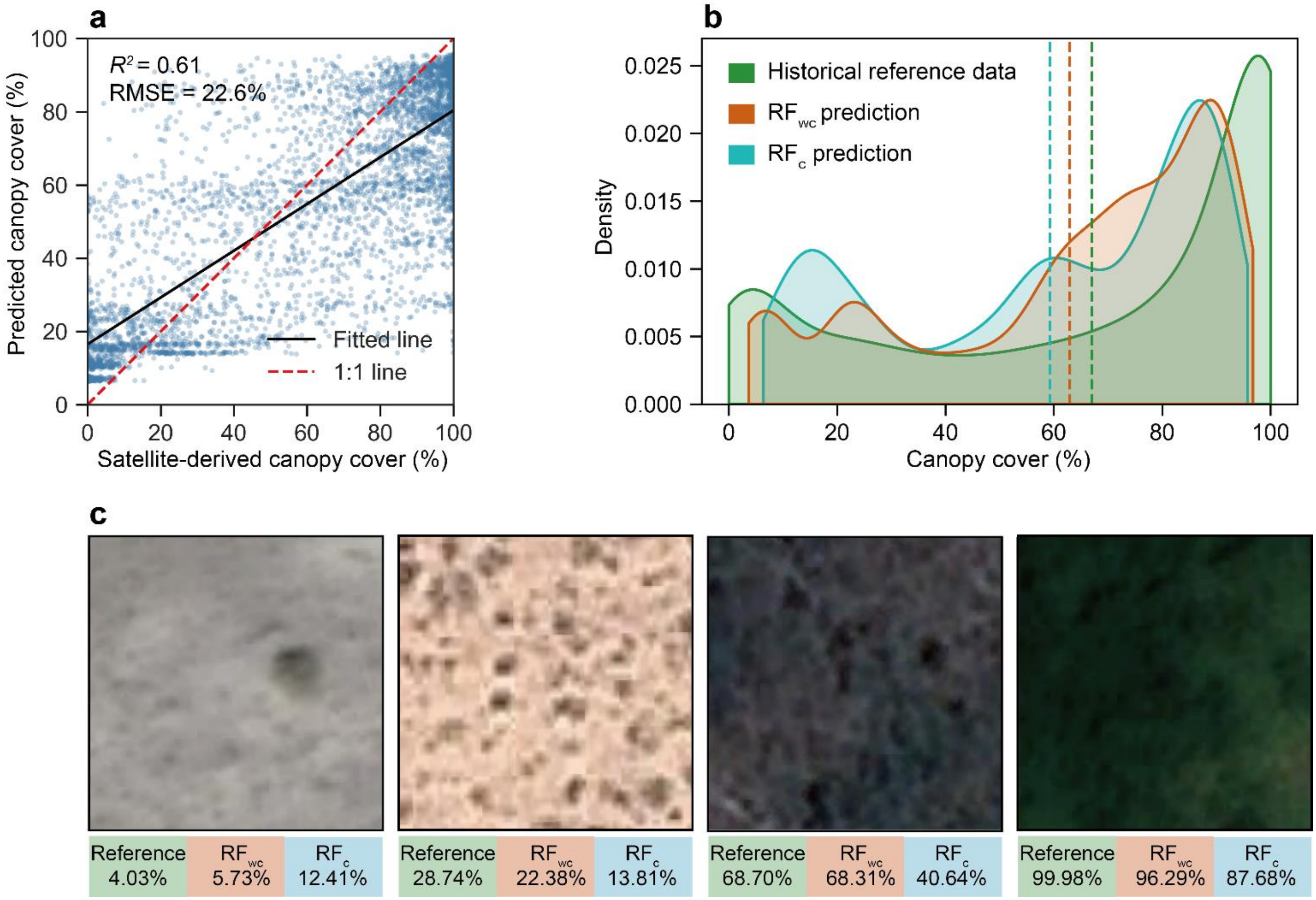

Fig. 10. (a) Assessment of temporal transferability for the RF model incorporating climatic features. (b) Kernel density distributions of canopy cover derived from historical reference data, the RF model without climatic variables (RF_{wc}), and the RF model with climatic variables (RF_c). Vertical dashed lines indicate the corresponding median values. (c) Comparison of grassland canopy cover estimates from different RF models across four representative regions.

4.2 Comparisons with existing grassland canopy cover products

To further evaluate the spatial fidelity and reliability of our estimates, we conducted a comparative analysis with three established canopy cover datasets, including the 30 m MultiVI fractional vegetation cover (FVC) dataset (Zhao et al., 2023), the 250 m MODIS VCF product (DiMiceli et al., 2022), and the 250 m China FVC dataset (Gao et al., 2022) (Table S3). When evaluated against the historical validation dataset, our product achieved the highest predictive accuracy, significantly outperforming the existing datasets, which exhibited varying degrees of systematic bias (Fig. 4b and Fig. 11). For example, due to its coarse-resolution, the MODIS VCF product introduced pronounced mixed-pixel effects, leading to substantial underestimation in densely vegetated regions (R^2 = 0.26; Fig. 11a). Although the China FVC dataset operates at the same 250

https://doi.org/10.5194/essd-2026-628
Preprint. Discussion started: 10 August 2026

m resolution, it partially mitigated this high-density underestimation (R^2 = 0.56; Fig. 11b) by optimizing endmember parameters for Chinese ecosystems. Nevertheless, the coarse pixel size still resulted in considerable dispersion relative to our 30 m estimates. Despite matching our 30 m spatial resolution, the MultiVI FVC dataset failed to accurately capture canopy cover variability (R^2 = 0.06; Fig. 11c), exhibiting systematic underestimation across all vegetation density gradients, particularly in sparsely vegetated areas.

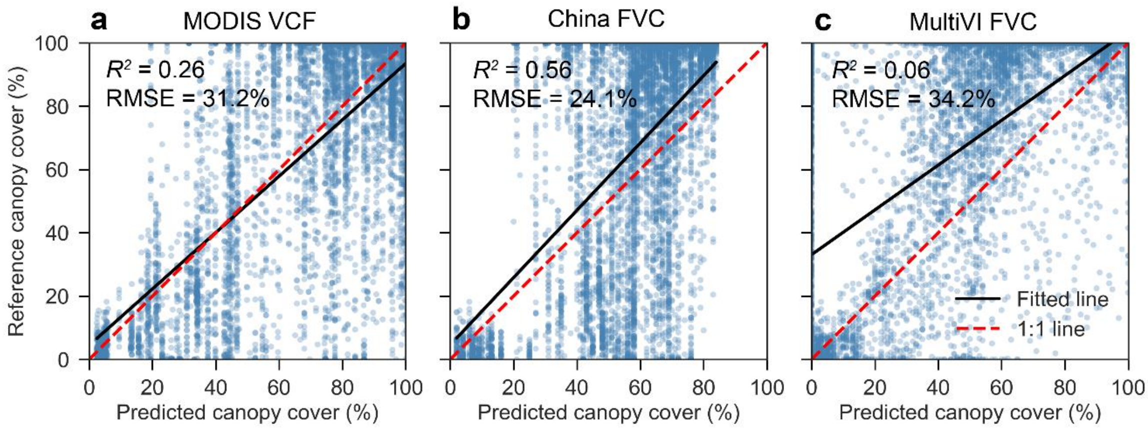

Fig. 11. Accuracy assessment of three existing products against the historical validation dataset. Scatter plots compare reference canopy cover with estimates from (a) the MODIS Vegetation Continuous Fields (MODIS VCF) product, (b) the China fractional vegetation cover (FVC) dataset, and (c) the MultiVI FVC dataset.

Visual inspection further corroborates the superiority of our dataset over existing products (Fig. 12). Compared with high-resolution Google Earth imagery, coarse-resolution products such as MODIS VCF and China FVC often miss the fine-scale spatial heterogeneity of complex terrains, particularly in alpine meadow (Fig. 12a) and typical steppe (Fig. 12e). Although the MultiVI FVC product also provides 30 m resolution, it exhibits noticeable residual sensor artifacts across diverse grassland types (Fig. 12b-d). In contrast, our dataset accurately delineates spatial gradients, complex topographic variations, and distinct boundaries of localized vegetation patches. By effectively mitigating historical sensor artifacts and leveraging high-resolution modeling, our dataset preserves high spatial fidelity, providing a more realistic representation of regional grassland ecosystems.

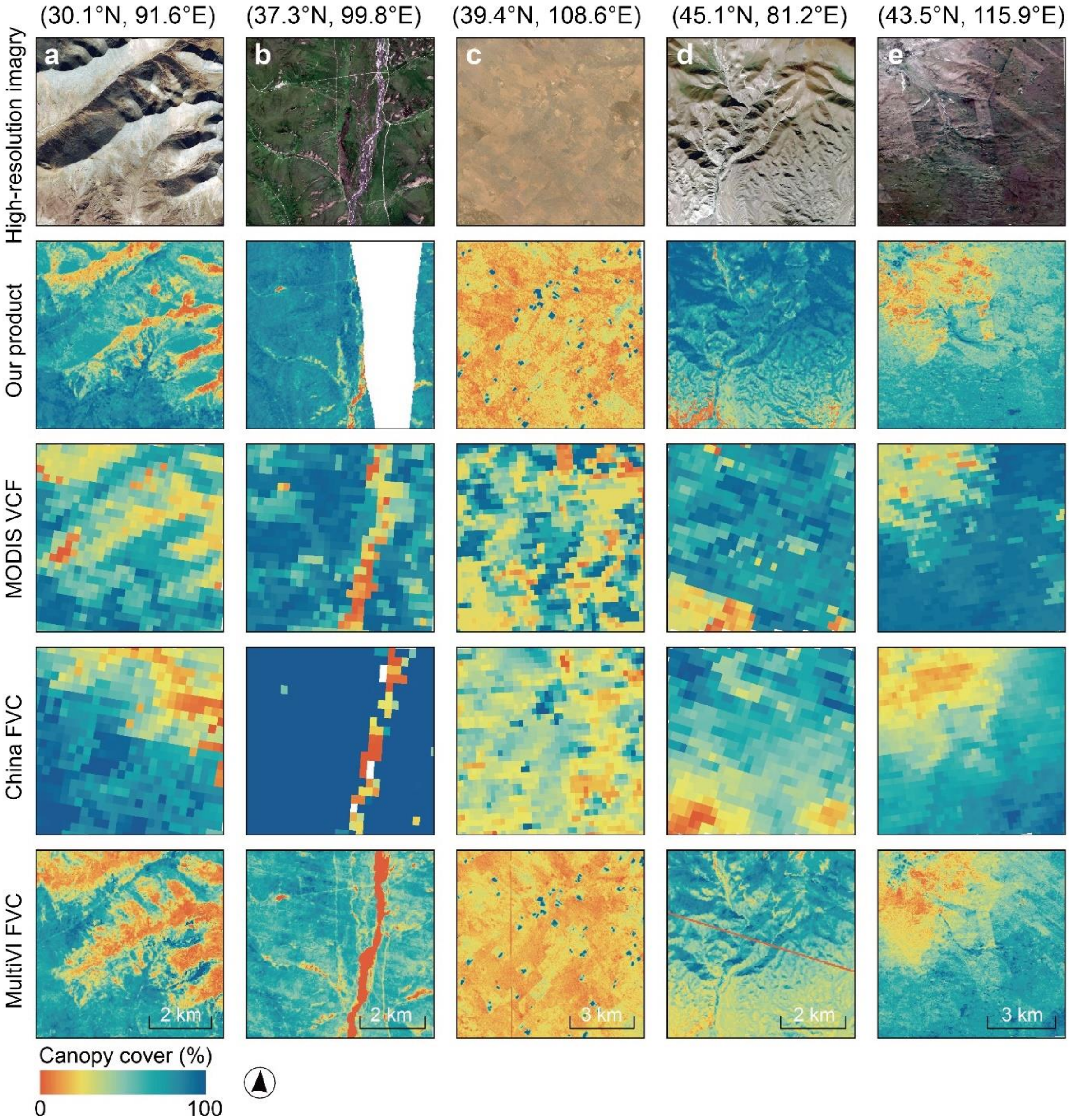

Fig. 12. Visual comparison of spatial details among different grassland canopy cover products across representative grassland types. Panels show (a) alpine meadow, (b) alpine steppe, (c) desert steppe, (d) meadow steppe, and (e) typical steppe. The top-row high-resolution imagery used as reference are (a) Imagery © 2026 Maxar Technologies, (b–d) Imagery © 2026 CNES/Airbus, (e) Imagery © 2026 Airbus derived from Google Earth Pro.

https://doi.org/10.5194/essd-2026-628
Preprint. Discussion started: 10 August 2026

4.3 The drivers of canopy cover dynamics across China's grassland

China's main grassland area (57.16%) showed no significant change in canopy cover over the past three decades, while a substantial proportion (41.76%) experienced a statistically significant increase. In contrast, only a small fraction (1.08%) showed a significant decline (Fig. 7a, b). Despite the predominance of nonsignificant trends, the widespread canopy cover increase is consistent with the general greening reported previously (Liu et al., 2023; Piao et al., 2019). SHAP-based analysis further indicates that these large-scale dynamics are primarily driven by climatic factors, particularly drought, precipitation, and temperature (Fig. 8a). Notably, drought and precipitation together dominate the ecological trajectories of nearly 80% of China's grasslands (Fig. 8b), highlighting the critical role of water availability. These climate-driven patterns are especially pronounced across the Qinghai–Tibet Plateau, Xinjiang, and the Loess Plateau (Fig. 8b). Over the past three decades, these regions have generally experienced increased precipitation and alleviated drought stress (Fig. S4 and Fig. S5), which have substantially contributed to the observed increases in grassland canopy cover (Fig. 8a, b). In contrast, Inner Mongolia has experienced persistent droughts (Fig. S4), resulting in stable or even declining canopy cover trends (Fig. 7c).

Although anthropogenic factors exert a relatively limited influence on long-term grassland dynamics at the national scale (Fig. 8b), intensive human activities can dominate in localized regions. For example, in parts of northern Xinjiang and the southeastern Qinghai-Tibet Plateau, canopy cover has remained stable despite comparable climatic amelioration (Fig. S4 and Fig. S5), suggesting that anthropogenic pressures have overridden climate as the primary drivers. In contrast, northeastern Inner Mongolia exhibits a significant increase in canopy cover despite intensified grazing activity and higher HMI values (Fig. S7 and Fig. S8), likely reflecting the effectiveness of ecological conservation policies in promoting grassland recovery. Overall, while anthropogenic factors can govern grassland dynamics at local scales, drought remains the dominant driver across most grassland ecosystems. As droughts are projected to grow more frequent and severe under future climate change (Chen et al., 2025), integrating drought risk mitigation with sustainable grazing management and ecological restoration into adaptive policy frameworks will be critical for safeguarding grassland ecosystems.

4.4 The uncertainty and limitations of the canopy cover dataset

To characterize the uncertainty of the canopy cover product, we quantified per-pixel uncertainty for 2021 as the standard deviation of predictions across the five-fold cross-validation ensemble. Across all grassland pixels, the uncertainty of the canopy cover dataset was heterogeneously distributed (Fig. 13a), averaging 2.25% (standard deviation = 0.51%) and following a narrow, unimodal distribution in which most pixels fell between roughly 1% and 4% (Fig. 13b). Based on the three representative regions, we identified three major sources of uncertainty (Fig. 13c-e). First, intense human activity can substantially increase uncertainty. In the agriculture-grassland transitional zone of northeastern Inner Mongolia (Fig. 13c), for example, frequent cultivation, grazing, and land management amplify the interannual variability of grassland condition, making it difficult for the model to produce stable and consistent predictions and thereby elevating uncertainty. A similar pattern occurs in other regions of strong human activity (Fig. S8), such as the Loess Plateau and southern Xinjiang (Fig. 13a).

https://doi.org/10.5194/essd-2026-628
Preprint. Discussion started: 10 August 2026

Second, data quality limitations of the early Landsat missions also contribute to uncertainty. In western China, such as northwestern Qinghai-Tibet Plateau (Fig. 13d), limited observations and sensor anomalies meant that the RF model was trained and applied on fewer high-quality inputs, thereby increasing the uncertainty of the predictions. Third, topographic heterogeneity further elevates uncertainty. In high-mountain regions, such as the Tianshan and Altai ranges of northern Xinjiang (Fig. 13e), grassland canopy cover varies sharply with elevation and aspect, producing pronounced differences over short distances and, consequently, higher pixel-level prediction uncertainty. The same pattern is evident on the Qinghai-Tibet Plateau, where alpine meadows and alpine steppes dominate. These uncertainties should be taken into account in further applications. When using this dataset for pixel-level analyses over the these high-uncertainty regions—zones of intense human activity, western areas with sparse Landsat coverage, and topographically complex high-mountain terrain—users should carefully evaluate whether these uncertainty and residual issues could influence their results.

https://doi.org/10.5194/essd-2026-628
Preprint. Discussion started: 10 August 2026

Earth System Science Data
Open Access
Discussions

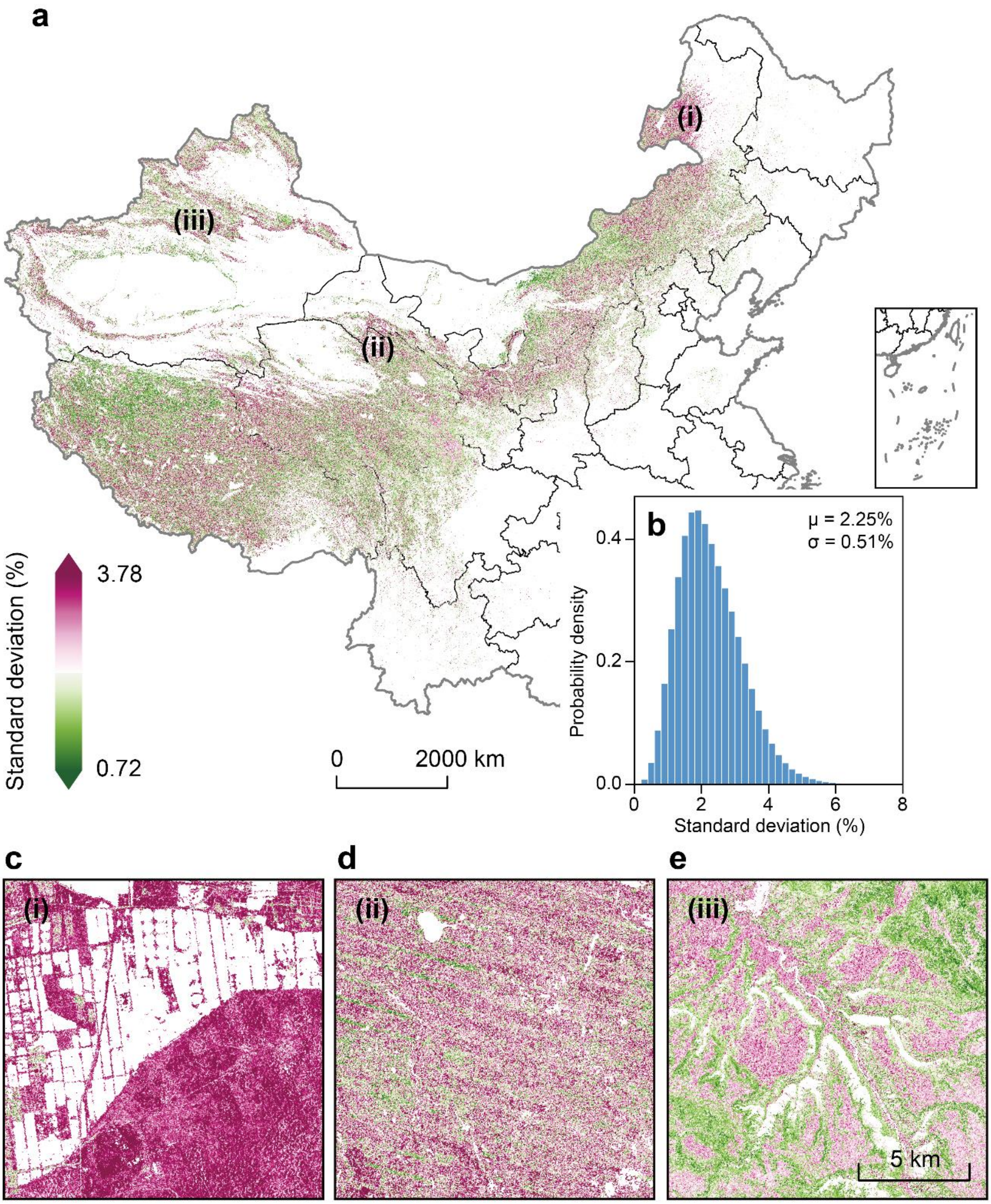

Fig. 13. Per-pixel uncertainty of the 2021 grassland canopy cover estimates, quantified as the standard deviation across the five-fold cross-validation ensemble. (a) Spatial distribution of the uncertainty across China. (b) Histogram of the uncertainty values. (c–e) Close-up views of three representative regions.

https://doi.org/10.5194/essd-2026-628
Preprint. Discussion started: 10 August 2026

Furthermore, the study has limitations. First, the spatiotemporal distribution of historical validation sites remains limited, particularly during the early years of the time series and within alpine grassland. For example, the earliest available validation sites dated only to 2002, and alpine steppe was represented by just two sites. Such sparse coverage may weaken the robustness of temporal transferability assessments. As more field observation datasets become publicly available, the validation database can be expanded to alleviate this limitation. Second, despite using all available Landsat observations and implementing rigorous quality control methods, limited sensor coverage, low acquisition frequency still caused missing data and subtle striping artifacts in some year scenes, especially in the western region. Recent advances demonstrating a global 30 m daily seamless reflectance data cube (Chen et al., 2024) provide a promising alternative for addressing such persistent data quality limitations. Third, this study revealed the dynamics of grassland canopy cover over the past three decades, relying solely on linear regression models to evaluate long-term dynamics may oversimplify the complex, non-linear processes. Grassland ecosystems frequently exhibit non-linear responses to climatic fluctuations and anthropogenic disturbances (Berdugo et al., 2022), and simple linear analyses often fail to capture these complex trajectories. Therefore, future research should incorporate time-series breakpoint detection algorithms and trajectory analysis, which will facilitate a more comprehensive understanding of recovery resilience of large-scale grassland ecosystems.

5 Data availability

The national grassland canopy cover dataset generated in this study is archived on Zenodo and can be freely downloaded from https://doi.org/10.5281/zenodo.20301123 (Jiang et al., 2026). The dataset consists of 34 single-band GeoTIFF files containing year-by-year data from 1990 to 2023, with pixel values from 1 to 100 representing the percentage of annual peak grassland canopy cover per pixel; a value of 0 denotes no data value. Files use the naming format "xxxx.tif", where "xxxx" represents the year (e.g., 1990.tif corresponds to the peak grassland canopy cover of China in 1990). Because all files share the same spatial reference and 30 m resolution, they allow direct pixel-level comparison across years.

6 Conclusions

Here, we developed a high precision and robust temporal transferability RF regression model that integrates extensive multi-year drone imagery with multi-source remote sensing data to generate a 30 m wall-to-wall annual dataset of grassland canopy cover for China from 1990 to 2023. Based on this dataset, we characterized the spatiotemporal dynamics of grassland canopy cover over the past three decades. Spatially, the 34-year mean canopy cover was 43.80%, exhibiting a pronounced southeast-to-northwest decreasing gradient. Temporally, most grassland areas remained stable or showed significant increases, while only a small proportion experienced persistent declines. Among the driving factors, drought emerged as the dominant regulator of long-term grassland dynamics at the national scale, exerting a substantially stronger influence than precipitation, temperature, and anthropogenic factors. Overall, this dataset targets a broad user community, including grassland ecologists, remote-sensing scientists, and policymakers concerned with grassland conservation and sustainable management. Its spatially continuous, high-resolution national canopy cover information supports various applications, such as monitoring grassland degradation and recovery, guiding grazing and land-use management, and serving as a benchmark for validating other canopy cover products. As climate change intensifies and extreme events grow more frequent, it provides an essential basis for deepening insight into grassland ecosystem dynamics and for evidence-based conservation and management.

Supplement link

Additional supporting information can be found online in the Supporting Information section.

Author contributions

Xuanhao Jiang: Conceptualization, Methodology, Formal analysis, Data curation, Writing – original draft.

Tianyu Hu: Conceptualization, Methodology, Data curation, Funding acquisition, Investigation.

Yanjun Su: Conceptualization, Methodology, Formal analysis, Writing – original draft, Funding acquisition.

Zhenying Huang, Zhiyao Tang: Project administration.

Leiyi Chen, Wenli Chen, Xiaoli Cheng, Yunxiang Cheng, Yuejun Fan, Ruiru Gao, Tiangang Gao, Yanming Gong, Yanpei Guo, Xiaokang Hu, Chengjun Ji, Liping Li, Shijin Li, Guofang Liu, Wanyin Luo, Hongyuan Ma, Wenhong Ma, Xiujuan Qiao, Chuangye Song, Guoyan Wang, Lei Wang, Qinggang Wang, Yonghui Wang, Zhong Wang, Xuejun Yang, Yan Yang, Yongchuan Yang, Xuehua Ye, Chunying Yin, Feihai Yu, Pujin Zhang, Shuren Zhang, Chengyang Zheng, Luhong Zhou: Investigation.

All authors: Writing – review & editing.

Competing interests

The authors declare that they have no conflict of interest.

Financial support

This work was supported by the Strategic Priority Research Program of Chinese Academy of Sciences (Grant No. XDA26010101).

References

Andreatta, D., Gianelle, D., Scotton, M., and Dalponte, M.: Estimating grassland vegetation cover with remote sensing: A comparison between Landsat-8, Sentinel-2 and PlanetScope imagery, Ecol. Indic., 141, 109102, https://doi.org/10.1016/j.ecolind.2022.109102, 2022.

Bai, Y. and Cotrufo, M. F.: Grassland soil carbon sequestration: Current understanding, challenges, and solutions, Science, 377, 603–608, https://doi.org/10.1126/science.abo2380, 2022.

Bardgett, R. D., Bullock, J. M., Lavorel, S., Manning, P., Schaffner, U., Ostle, N., Chomel, M., Durigan, G., Fry, E. L., Johnson, D., Lavallee, J. M., Le Provost, G., Luo, S., Png, K., Sankaran, M., Hou, X., Zhou, H., Ma, L., Ren, W., Li, X., Ding, Y., Li, Y., and Shi, H.: Combatting global grassland degradation, Nat. Rev. Earth Environ., 2, 720–735, https://doi.org/10.1038/s43017-021-00207-2, 2021.

Baret, F., Weiss, M., Lacaze, R., Camacho, F., Makhmara, H., Pacholcyzk, P., and Smets, B.: GEOV1: LAI and FAPAR essential climate variables and FCOVER global time series capitalizing over existing products. Part 1: Principles of development and production, Remote Sens. Environ., 137, 299–309, https://doi.org/10.1016/j.rse.2012.12.027, 2013.

Barnett, V. and Lewis, T.: Outliers in statistical data, Wiley, New York, 1994.

Beguería, S., Vicente-Serrano, S. M., Reig, F., and Latorre, B.: Standardized precipitation evapotranspiration index (SPEI) revisited: Parameter fitting, evapotranspiration models, tools, datasets and drought monitoring, Int. J. Climatol., 34, 3001–3023, https://doi.org/10.1002/joc.3887, 2014.

Berdugo, M., Gaitán, J. J., Delgado-Baquerizo, M., Crowther, T. W., and Dakos, V.: Prevalence and drivers of abrupt vegetation shifts in global drylands, Proc. Natl. Acad. Sci. U.S.A., 119, e2123393119, https://doi.org/10.1073/pnas.2123393119, 2022.

Bian, J., Li, A., Zhang, Z., Zhao, W., Lei, G., Yin, G., Jin, H., Tan, J., and Huang, C.: Monitoring fractional green vegetation cover dynamics over a seasonally inundated alpine wetland using dense time series HJ-1A/B constellation images and an adaptive endmember selection LSMM model, Remote Sens. Environ., 197, 98–114, https://doi.org/10.1016/j.rse.2017.05.031, 2017.

Breiman, L.: Random forests, Mach. Learn., 45, 5–32, https://doi.org/10.1023/A:1010933404324, 2001.

Cai, Y., Xu, X., Zhu, P., Nie, S., Wang, C., Xiong, Y., and Liu, X.: Unveiling spatiotemporal tree cover patterns in China: The first 30 m annual tree cover mapping from 1985 to 2023, ISPRS J. Photogramm. Remote Sens., 216, 240–258, https://doi.org/10.1016/j.isprsjprs.2024.08.001, 2024.

Chen, J., Yi, S., Qin, Y., and Wang, X.: Improving estimates of fractional vegetation cover based on UAV in alpine grassland on the Qinghai–Tibetan Plateau, Int. J. Remote Sens., 37, 1922–1936, https://doi.org/10.1080/01431161.2016.1165884, 2016.

Chen, L., Brun, P., Buri, P., Fatichi, S., Gessler, A., McCarthy, M. J., Pellicciotti, F., Stocker, B., and Karger, D. N.: Global increase in the occurrence and impact of multiyear droughts, Science, 387, 278–284, https://doi.org/10.1126/science.ado4245, 2025.

Chen, S., Wang, J., Liu, Q., Liang, X., Liu, R., Qin, P., Yuan, J., Wei, J., Yuan, S., Huang, H., and Gong, P.: Global 30 m seamless data cube (2000–2022) of land surface reflectance generated from Landsat 5, 7, 8, and 9 and MODIS Terra constellations, Earth Syst. Sci. Data, 16, 5449–5475, https://doi.org/10.5194/essd-16-5449-2024, 2024.

Chen, T. and Guestrin, C.: XGBoost: A scalable tree boosting system, in: Proceedings of the 22nd ACM SIGKDD International Conference on Knowledge Discovery and Data Mining, ACM, San Francisco, CA, USA, pp. 785–794, https://doi.org/10.1145/2939672.2939785, 2016.

Daryaei, A., Sohrabi, H., Atzberger, C., and Immitzer, M.: Fine-scale detection of vegetation in semi-arid mountainous areas with focus on riparian landscapes using Sentinel-2 and UAV data, Comput. Electron. Agric., 177, 105686, https://doi.org/10.1016/j.compag.2020.105686, 2020.

DiMiceli, C., Sohlberg, R., and Townshend, J.: MODIS/Terra Vegetation Continuous Fields Yearly L3 Global 250m SIN Grid V061, NASA Land Processes Distributed Active Archive Center [data set], https://doi.org/10.5067/MODIS/MOD44B.061, 2022.

Dubayah, R., Blair, J. B., Goetz, S., Fatoyinbo, L., Hansen, M., Healey, S., Hofton, M., Hurtt, G., Kellner, J., Luthcke, S., Armston, J., Tang, H., Duncanson, L., Hancock, S., Jantz, P., Marselis, S., Patterson, P. L., Qi, W., and Silva, C.: The Global Ecosystem Dynamics Investigation: High-resolution laser ranging of the Earth's forests and topography, Sci. Remote Sens., 1, 100002, https://doi.org/10.1016/j.srs.2020.100002, 2020.

Dusseux, P., Hubert-Moy, L., Corpetti, T., and Vertès, F.: Evaluation of SPOT imagery for the estimation of grassland biomass, Int. J. Appl. Earth Obs. Geoinf., 38, 72–77, https://doi.org/10.1016/j.jag.2014.12.003, 2015.

Farr, T.G., Rosen, P. A., Caro, E., Crippen, R., Duren, R., Hensley, S., Kobrick, M., Paller, M., Rodriguez, E., Roth, L., Seal, D., Shaffer, S., Shimada, J., Umland, J., Werner, M., Oskin, M., Burbank, D., and Alsdorf, D.: The Shuttle Radar Topography Mission, Rev. Geophys., 45, 2005RG000183, https://doi.org/10.1029/2005RG000183, 2007.

Gao, B.: NDWI—A normalized difference water index for remote sensing of vegetation liquid water from space, Remote Sens. Environ., 58, 257–266, https://doi.org/10.1016/S0034-4257(96)00067-3, 1996.

Gao, J., Shi, Y., Zhang, H., Chen, X., Zhang, W., Shen, W., Xiao, T., and Zhang, Y.: China regional 250m fractional vegetation cover data set (2000-2024), National Tibetan Plateau Data Center [data set], https://doi.org/10.11888/Terre.tpdc.300330, 2022.

Gao, L., Wang, X., Johnson, B. A., Tian, Q., Wang, Y., Verrelst, J., Mu, X., and Gu, X.: Remote sensing algorithms for estimation of fractional vegetation cover using pure vegetation index values: A review, ISPRS J. Photogramm. Remote Sens., 159, 364–377, https://doi.org/10.1016/j.isprsjprs.2019.11.018, 2020.

Ge, J., Meng, B., Liang, T., Feng, Q., Gao, J., Yang, S., Huang, X., and Xie, H.: Modeling alpine grassland cover based on MODIS data and support vector machine regression in the headwater region of the Huanghe River, China, Remote Sens. Environ., 218, 162–173, https://doi.org/10.1016/j.rse.2018.09.019, 2018.

Gessner, U., Machwitz, M., Conrad, C., and Dech, S.: Estimating the fractional cover of growth forms and bare surface in savannas. A multi-resolution approach based on regression tree ensembles, Remote Sens. Environ., 129, 90–102, https://doi.org/10.1016/j.rse.2012.10.026, 2013.

Gitelson, A. and Merzlyak, M. N.: Quantitative estimation of chlorophyll-a using reflectance spectra: Experiments with autumn chestnut and maple leaves, J. Photochem. Photobiol. B: Biol., 22, 247–252, https://doi.org/10.1016/1011-1344(93)06963-4, 1994.

Glenn, E. P., Huete, A. R., Nagler, P. L., and Nelson, S. G.: Relationship between remotely-sensed vegetation indices, canopy attributes and plant physiological processes: What vegetation indices can and cannot tell us about the landscape, Sensors, 8, 2136–2160, https://doi.org/10.3390/s8042136, 2008.

Hatfield, J. L., Kanemasu, E. T., Asrar, G., Jackson, R. D., Pinter, P. J., Reginato, R. J., and Idso, S. B.: Leaf-area estimates from spectral measurements over various planting dates of wheat, Int. J. Remote Sens., 6, 167–175, https://doi.org/10.1080/01431168508948432, 1985.

Holben, B. N.: Characteristics of maximum-value composite images from temporal AVHRR data, Int. J. Remote Sens., 7, 1417–1434, https://doi.org/10.1080/01431168608948945, 1986.

Hu, T., Cao, M., Zhao, X., Liu, X., Liu, Z., Liu, L., Huang, Z., Tao, S., Tang, Z., Guo, Y., Ji, C., Zheng, C., Wang, G., Hu, X., Zhou, L., Cheng, Y., Ma, W., Wang, Y., Zhang, P., Fan, Y., Yu, F., Wang, Z., Qiao, X., Cheng, X., Yin, C., Ma, H., Li, L., Yang, Y., Luo, W., Gong, Y., Wang, L., Chen, L., Liu, G., Song, C., Yang, X., Ye, X., Zhang, S., Zhu, X., Wang, Q., Li, S., Yang, Y., Liu, L., Kelly, M., Fang, J., and Su, Y.: High-resolution mapping of grassland canopy cover in China through the integration of extensive drone imagery and satellite data, ISPRS J. Photogramm. Remote Sens., 218, 69–83, https://doi.org/10.1016/j.isprsjprs.2024.09.004, 2024.

Huete, A., Didan, K., Miura, T., Rodriguez, E. P., Gao, X., and Ferreira, L. G.: Overview of the radiometric and biophysical performance of the MODIS vegetation indices, Remote Sens. Environ., 83, 195–213, https://doi.org/10.1016/S0034-4257(02)00096-2, 2002.

Huete, A. R.: A soil-adjusted vegetation index (SAVI), Remote Sens. Environ., 25, 295–309, https://doi.org/10.1016/0034-4257(88)90106-X, 1988.

Hunt Jr., E. and Rock, B.: Detection of changes in leaf water content using near- and middle-infrared reflectances, Remote Sens. Environ., 30, 43–54, https://doi.org/10.1016/0034-4257(89)90046-1, 1989.

Jiang, X., Hu, T., Huang, Z., Tang, Z., Chen, L., Chen, W., Cheng, X., Cheng, Y., Fan, Y., Gao, R., Gao, T., Gong, Y., Guo, Y., Hu, X., Ji, C., Li, L., Li, S., Liu, G., Luo, W., Ma, H., Ma, W., Qiao, X., Song, C., Wang, G., Wang, L., Wang, Q., Wang, Y., Wang, Z., Yang, X., Yang, Y., Yang, Y., Ye, X., Yin, C., Yu, F., Zhang, P., Zhang, S., Zheng, C., Zhou, L., and Su, Y.: Annual 30 m grassland canopy cover dataset for China from 1990 to 2023, Zenodo [data set], https://doi.org/10.5281/zenodo.20301123, 2026.

Jones, H. P., Jones, P. C., Barbier, E. B., Blackburn, R. C., Rey Benayas, J. M., Holl, K. D., McCrackin, M., Meli, P., Montoya, D., and Mateos, D. M.: Restoration and repair of Earth's damaged ecosystems, Proc. R. Soc. B, 285, 20172577, https://doi.org/10.1098/rspb.2017.2577, 2018.

https://doi.org/10.5194/essd-2026-628
Preprint. Discussion started: 10 August 2026

Kennedy, C.M., Oakleaf, J. R., Theobald, D. M., Baruch-Mordo, S., and Kiesecker, J.: Managing the middle: A shift in conservation priorities based on the global human modification gradient, Glob. Chang. Biol., 25, 811–826, https://doi.org/10.1111/gcb.14549, 2019.

Lehnert, L. W., Meyer, H., Wang, Y., Miehe, G., Thies, B., Reudenbach, C., and Bendix, J.: Retrieval of grassland plant coverage on the Tibetan Plateau based on a multi-scale, multi-sensor and multi-method approach, Remote Sens. Environ., 164, 197–207, https://doi.org/10.1016/j.rse.2015.04.020, 2015.

Lewińska, K. E., Okujeni, A., Kowalski, K., Lehmann, F., Radeloff, V. C., Leser, U., and Hostert, P.: Impact of data density and endmember definitions on long-term trends in ground cover fractions across European grasslands, Remote Sens. Environ., 323, 114736, https://doi.org/10.1016/j.rse.2025.114736, 2025.

Li, X.-B., Chen, Y.-H., Yang, H., and Zhang, Y.-X.: Improvement, comparison, and application of field measurement methods for grassland vegetation fractional coverage, J. Integr. Plant Biol., 47, 1074–1083, https://doi.org/10.1111/j.1744-7909.2005.00134.x, 2005.

Liu, L., Zheng, J., Guan, J., Han, W., and Liu, Y.: Grassland cover dynamics and their relationship with climatic factors in China from 1982 to 2021, Sci. Total Environ., 905, 167067, https://doi.org/10.1016/j.scitotenv.2023.167067, 2023.

Louppe, G., Wehenkel, L., Sutera, A., and Geurts, P.: Understanding variable importances in forests of randomized trees, in: Advances in Neural Information Processing Systems, Curran Associates, Inc., 2013.

Lyu, X., Li, X., Dang, D., Dou, H., Wang, K., and Lou, A.: Unmanned Aerial Vehicle (UAV) remote sensing in grassland ecosystem monitoring: A systematic review, Remote Sens., 14, 1096, https://doi.org/10.3390/rs14051096, 2022.

Maestre, F. T., Le Bagousse-Pinguet, Y., Delgado-Baquerizo, M., Eldridge, D. J., Saiz, H., Berdugo, M., Gozalo, B., Ochoa, V., Guirado, E., García-Gómez, M., Valencia, E., Gaitán, J. J., Asensio, S., Mendoza, B. J., Plaza, C., Díaz-Martínez, P., Rey, A., Hu, H.-W., He, J.-Z., Wang, J.-T., Lehmann, A., Rillig, M. C., Cesarz, S., Eisenhauer, N., Martínez-Valderrama, J., Moreno-Jiménez, E., Sala, O., Abedi, M., Ahmadian, N., Alados, C. L., Aramayo, V., Amghar, F., Arredondo, T., Ahumada, R. J., Bahalkeh, K., Ben Salem, F., Blaum, N., Boldgiv, B., Bowker, M. A., Bran, D., Bu, C., Canessa, R., Castillo-Monroy, A. P., Castro, H., Castro, I., Castro-Quezada, P., Chibani, R., Conceição, A. A., Currier, C. M., Darrouzet-Nardi, A., Deák, B., Donoso, D. A., Dougill, A. J., Durán, J., Erdenetsetseg, B., Espinosa, C. I., Fajardo, A., Farzam, M., Ferrante, D., Frank, A. S. K., Fraser, L. H., Gherardi, L. A., Greenville, A. C., Guerra, C. A., Gusmán-Montalvan, E., Hernández-Hernández, R. M., Hölzel, N., Huber-Sannwald, E., Hughes, F. M., Jadán-Maza, O., Jeltsch, F., Jentsch, A., Kaseke, K. F., Köbel, M., Koopman, J. E., Leder, C. V., Linstädter, A., le Roux, P. C., Li, X., Liancourt, P., Liu, J., Louw, M. A., Maggs-Kölling, G., Makhalanyane, T. P., Issa, O. M., Manzaneda, A. J., Marais, E., Mora, J. P., Moreno, G., Munson, S. M., Nunes, A., Oliva, G., Oñatibia, G. R., Peter, G., Pivari, M. O. D., Pueyo, Y., Quiroga, R. E., Rahmanian, S., Reed, S. C., et al.: Grazing and ecosystem service delivery in global drylands, Science, 378, 915–920, https://doi.org/10.1126/science.abq4062, 2022.

https://doi.org/10.5194/essd-2026-628
Preprint. Discussion started: 10 August 2026

Mersha, M., Lam, K., Wood, J., AlShami, A. K., and Kalita, J.: Explainable artificial intelligence: A survey of needs, techniques, applications, and future direction, Neurocomputing, 599, 128111, https://doi.org/10.1016/j.neucom.2024.128111, 2024.

Muñoz-Sabater, J., Dutra, E., Agustí-Panareda, A., Albergel, C., Arduini, G., Balsamo, G., Boussetta, S., Choulga, M., Harrigan, S., Hersbach, H., Martens, B., Miralles, D. G., Piles, M., Rodríguez-Fernández, N. J., Zsoter, E., Buontempo, C., and Thépaut, J.-N.: ERA5-Land: A state-of-the-art global reanalysis dataset for land applications, Earth Syst. Sci. Data, 13, 4349–4383, https://doi.org/10.5194/essd-13-4349-2021, 2021.

Piao, S., Wang, X., Park, T., Chen, C., Lian, X., He, Y., Bjerke, J. W., Chen, A., Ciais, P., Tømmervik, H., Nemani, R. R., and Myneni, R. B.: Characteristics, drivers and feedbacks of global greening, Nat. Rev. Earth Environ., 1, 14–27, https://doi.org/10.1038/s43017-019-0001-x, 2019.

Pywell, R. F., Meek, W. R., Webb, N. R., Putwain, P. D., and Bullock, J. M.: Long-term heathland restoration on former grassland: The results of a 17-year experiment, Biol. Conserv., 144, 1602–1609, https://doi.org/10.1016/j.biocon.2011.02.010, 2011.

Roy, D. P., Kovalskyy, V., Zhang, H. K., Vermote, E. F., Yan, L., Kumar, S. S., and Egorov, A.: Characterization of Landsat-7 to Landsat-8 reflective wavelength and normalized difference vegetation index continuity, Remote Sens. Environ., 185, 57–70, https://doi.org/10.1016/j.rse.2015.12.024, 2016.

Smith, M. D., Wilkins, K. D., Holdrege, M. C., Wilfahrt, P., Collins, S. L., Knapp, A. K., Sala, O. E., Dukes, J. S., Phillips, R. P., Yahdjian, L., Gherardi, L. A., Ohlert, T., Beier, C., Fraser, L. H., Jentsch, A., Loik, M. E., Maestre, F. T., Power, S. A., Yu, Q., Felton, A. J., Munson, S. M., Luo, Y., Abdoli, H., Abedi, M., Alados, C. L., Alberti, J., Alon, M., An, H., Anacker, B., Anderson, M., Auge, H., Bachle, S., Bahalkeh, K., Bahn, M., Batbaatar, A., Bauerle, T., Beard, K. H., Behn, K., Beil, I., Biancari, L., Blindow, I., Bondaruk, V. F., Borer, E. T., Bork, E. W., Bruschetti, C. M., Byrne, K. M., Cahill Jr., J. F., Calvo, D. A., Carbognani, M., Cardoni, A., Carlyle, C. N., Castillo-Garcia, M., Chang, S. X., Chieppa, J., Cianciaruso, M. V., Cohen, O., Cordeiro, A. L., Cusack, D. F., Dahlke, S., Daleo, P., D’Antonio, C. M., Dietterich, L. H., Doherty, T. S., Dubbert, M., Ebeling, A., Eisenhauer, N., Fischer, F. M., Forte, T. G. W., Gebauer, T., Gozalo, B., Greenville, A. C., Guidoni-Martins, K. G., Hannusch, H. J., Vatsø Haugum, S., Hautier, Y., Hefting, M., Henry, H. A. L., Hoss, D., Ingrisch, J., Iribarne, O., Isbell, F., Johnson, Y., Jordan, S., Kelly, E. F., Kimmel, K., Kreyling, J., Kröel-Dulay, G., Kröpfl, A., Kübert, A., Kulmatiski, A., Lamb, E. G., Larsen, K. S., Larson, J., Lawson, J., Leder, C. V., Linstädter, A., Liu, J., Liu, S., Lodge, A. G., Longo, G., Loydi, A., Luan, J., Lubbe, F. C., Macfarlane, C., Mackie-Haas, K., Malyshev, A. V., Maturano-Ruiz, A., Merchant, T., Metcalfe, D. B., Mori, A. S., Mudongo, E., Newman, G. S., Nielsen, U. N., Nimmo, D., Niu, Y., Nobre, P., O’Connor, R. C., Ogaya, R., Oñatibia, G. R., Orbán, I., Osborne, B., Otfinowski, R., Pärtel, M., Penuelas, J., Peri, P. L., Peter, G., Petraglia, A., Picon-Cochard, C., Pillar, V. D., Piñeiro-Guerra, J.M., Ploughe, L.W., Plowes, R.M., Portales-Reyes, C., Prober, S.M., Pueyo, Y., Reed, S.C., Ritchie, E.G., Rodríguez, D.A., Rogers, W.E., Roscher, C., Sánchez, A.M., Santos, B.A., Scarfó, M.C., Seabloom, E.W., Shi, B., Souza, L., Stampfli, A., Standish, R.J., Sternberg, M., Sun, W., Sünnemann, M., Tedder, M., Thorvaldsen, P., Tian, D., Tielbörger, K., Valdecantos, A., Van Den Brink, L., Vandvik, V., Vankoughnett, M.R., Velle, L.G., Wang, C., Wang, Y., Wardle, G.M., Werner, C., Wei, C., Wiehl, G., Williams, J.L., Wolf, A.A., Zeiter, M., Zhang, F., Zhu, J., Zong, N., and Zuo, X.: Extreme drought impacts have been underestimated in grasslands and shrublands globally, Proc. Natl. Acad. Sci. U.S.A., 121, e2309881120, https://doi.org/10.1073/pnas.2309881120, 2024.

Song, J., Wan, S., Zhang, K., Hong, S., Xia, J., Piao, S., Wang, Y.-P., Chen, J., Hui, D., Luo, Y., Niu, S., Ru, J., Xu, H., Zheng, M., Liu, W., Wang, H., Tan, M., Zhou, Z., Feng, J., and Qiu, X.: Ecological restoration enhances dryland carbon stock by reducing surface soil carbon loss due to wind erosion, Proc. Natl. Acad. Sci. U.S.A., 121, e2416281121, https://doi.org/10.1073/pnas.2416281121, 2024.

Su, Y., Guo, Q., Hu, T., Guan, H., Jin, S., An, S., Chen, X., Guo, K., Hao, Z., Hu, Y., Huang, Y., Jiang, M., Li, J., Li, Z., Li, X., Li, X., Liang, C., Liu, R., Liu, Q., Ni, H., Peng, S., Shen, Z., Tang, Z., Tian, X., Wang, X., Wang, R., Xie, Z., Xie, Y., Xu, X., Yang, X., Yang, Y., Yu, L., Yue, M., Zhang, F., and Ma, K.: An updated Vegetation Map of China (1:1000000), Sci. Bull., 65, 1125–1136, https://doi.org/10.1016/j.scib.2020.04.004, 2020.

Taddei, R.: Maximum Value Interpolated (MVI): A maximum value composite method improvement in vegetation index profiles analysis, Int. J. Remote Sens., 18, 2365–2370, https://doi.org/10.1080/014311697217657, 1997.

Theobald, D. M., Oakleaf, J. R., Moncrieff, G., Voigt, M., Kiesecker, J., and Kennedy, C. M.: Global extent and change in human modification of terrestrial ecosystems from 1990 to 2022, Sci. Data, 12, 606, https://doi.org/10.1038/s41597-025-04892-2, 2025.

Tilman, D., Reich, P. B., Knops, J., Wedin, D., Mielke, T., and Lehman, C.: Diversity and productivity in a long-term grassland experiment, Science, 294, 843–845, https://doi.org/10.1126/science.1060391, 2001.

Tucker, C. J.: Red and photographic infrared linear combinations for monitoring vegetation, Remote Sens. Environ., 8, 127–150, https://doi.org/10.1016/0034-4257(79)90013-0, 1979.

Vicente-Serrano, S. M., Beguería, S., and López-Moreno, J. I.: A multiscalar drought index sensitive to global warming: The Standardized Precipitation Evapotranspiration Index, J. Clim., 23, 1696–1718, https://doi.org/10.1175/2009JCLI2909.1, 2010.

Wang, D., Peng, Q., Li, X., Zhang, W., Xia, X., Qin, Z., Ren, P., Liang, S., and Yuan, W.: A long-term high-resolution dataset of grasslands grazing intensity in China, Sci. Data, 11, 1194, https://doi.org/10.1038/s41597-024-04045-x, 2024.

Wang, Y., Lv, W., Xue, K., Wang, S., Zhang, L., Hu, R., Zeng, H., Xu, X., Li, Y., Jiang, L., Hao, Y., Du, J., Sun, J., Dorji, T., Piao, S., Wang, C., Luo, C., Zhang, Z., Chang, X., Zhang, M., Hu, Y., Wu, T., Wang, J., Li, B., Liu, P., Zhou, Y., Wang, A., Dong, S., Zhang, X., Gao, Q., Zhou, H., Shen, M., Wilkes, A., Miehe, G., Zhao, X., and Niu, H.: Grassland changes and adaptive management on the Qinghai–Tibetan Plateau, Nat. Rev. Earth Environ., 3, 668–683, https://doi.org/10.1038/s43017-022-00330-8, 2022.

Wiens, J. A.: Spatial scaling in ecology, Funct. Ecol., 3, 385, https://doi.org/10.2307/2389612, 1989.

Woodcock, C. E. and Strahler, A. H.: The factor of scale in remote sensing, Remote Sens. Environ., 21, 311–332, https://doi.org/10.1016/0034-4257(87)90015-0, 1987.

https://doi.org/10.5194/essd-2026-628
Preprint. Discussion started: 10 August 2026

Wulder, M. A., White, J. C., Goward, S. N., Masek, J. G., Irons, J. R., Herold, M., Cohen, W. B., Loveland, T. R., and Woodcock, C. E.: Landsat continuity: Issues and opportunities for land cover monitoring, Remote Sens. Environ., 112, 955–969, https://doi.org/10.1016/j.rse.2007.07.004, 2008.

Xiao, J. and Moody, A.: A comparison of methods for estimating fractional green vegetation cover within a desert-to-upland transition zone in central New Mexico, USA, Remote Sens. Environ., 98, 237–250, https://doi.org/10.1016/j.rse.2005.07.011, 2005.

Yang, J. and Huang, X.: The 30 m annual land cover dataset and its dynamics in China from 1990 to 2019, Earth Syst. Sci. Data, 13, 3907–3925, https://doi.org/10.5194/essd-13-3907-2021, 2021.

You, C., Chen, S., Tu, Z., Bian, C., Cui, E., Huang, K., Wan, F., Ping, J., Wei, N., and Xia, J.: Decadal trends in global grassland growth peaks and their drivers since the 1980s, Nat. Commun., 16, 9501, https://doi.org/10.1038/s41467-025-64565-x, 2025.

Yuan, X., Wang, Y., Ji, P., Wu, P., Sheffield, J., and Otkin, J. A.: A global transition to flash droughts under climate change, Science, 380, 187–191, https://doi.org/10.1126/science.abn6301, 2023.

Zhang, H., Tang, Z., Wang, B., Kan, H., Sun, Y., Qin, Y., Meng, B., Li, M., Chen, J., Lv, Y., Zhang, J., Niu, S., and Yi, S.: A 250 m annual alpine grassland AGB dataset over the Qinghai–Tibet Plateau (2000–2019) in China based on in situ measurements, UAV photos, and MODIS data, Earth Syst. Sci. Data, 15, 821–846, https://doi.org/10.5194/essd-15-821-2023, 2023.

Zhao, T., Mu, X., Song, W., Liu, Y., Xie, Y., Zhong, B., Xie, D., Jiang, L., and Yan, G.: Mapping spatially seamless fractional vegetation cover over China at a 30-m resolution and semimonthly intervals in 2010–2020 based on Google Earth Engine, J. Remote Sens., 3, https://doi.org/10.34133/remotesensing.0101, 2023.

Zhou, Y., Batelaan, O., Guan, H., Liu, T., Duan, L., Wang, Y., and Li, X.: Assessing long-term trends in vegetation cover change in the Xilin River Basin: Potential for monitoring grassland degradation and restoration, J. Environ. Manage., 349, 119579, https://doi.org/10.1016/j.jenvman.2023.119579, 2024.

Zhu, Z., Wang, S., and Woodcock, C. E.: Improvement and expansion of the Fmask algorithm: Cloud, cloud shadow, and snow detection for Landsats 4–7, 8, and Sentinel 2 images, Remote Sens. Environ., 159, 269–277, https://doi.org/10.1016/j.rse.2014.12.014, 2015.